macromol

MDPI

Article

Photopolymerized Gelatin–PNIPAM as Injectable Hydrogel Drug Delivery Systems

Olga Luneva [1], Eugene Sivtsov [2], Irina Bagriy [1], Olga Solomakha [1], Yulia Nashchekina [3], Alexey Nikiforov [1], Valeria Ibragimova [1] and Evgenia Korzhikova-Vlakh [1,4,*]

[1] Branch of Petersburg Nuclear Physics Institute Named by B.P. Konstantinov of National Research Centre "Kurchatov Institute"—Institute of Macromolecular Compounds, St. Petersburg 199004, Russia; olya.lun.1995@gmail.com (O.L.); bagriy240398@gmail.com (I.B.); solomanya@bk.ru (O.S.); anikiforov71@gmail.com (A.N.); vneterebskaya@list.ru (V.I.)
[2] Physical Chemistry Department, Saint-Petersburg State Institute of Technology (Technical University), St. Petersburg 190013, Russia; pjeka@yahoo.fr
[3] Institute of Cytology, Russian Academy of Sciences, St. Petersburg 194064, Russia; ulychka@mail.ru
[4] Institute of Chemistry, St. Petersburg State University, St. Petersburg 199034, Russia
* Correspondence: vlakh@hq.macro.ru

Abstract

Injectable hydrogels have attracted substantial and rapidly growing interest due to their ability to be administered into cavities of any shape and provide local therapeutic treatment. This study reports the synthesis and characterization of thermosensitive microgels and hydrogels obtained via photoinitiated copolymerization of methacrylated gelatin (GN-MA) and *N*-isopropylacrylamide (NIPAM) in the absence and presence of *N*,*N*′-methylenebisacrylamide (MBA). The effects of monomer concentration, crosslinker content (MBA), and irradiation time on product yield, grafted chain length, and material properties were systematically investigated. Depending on the polymerization conditions, microgel samples exhibited hydrodynamic diameters in the range of 354–1022 nm at 20 °C, which decreased to 183–308 nm upon heating to 40 °C. Freeze-drying of the microgel dispersions resulted in the formation of a porous sponge-like structure with pore sizes of 50–90 μm. Rheological studies of the hydrogel properties demonstrated evident thermoresponsive behavior, with storage moduli (G') ranging from 20 to 600 Pa, matching the mechanics of certain soft tissues. The hydrogels showed high equilibrium swelling capacity at 20 °C, which was reduced at 40 °C, as well as temperature-dependent moxifloxacin release (38–88% over 6 days) and excellent biocompatibility (>85% cell viability) with human skin fibroblasts. These findings make them promising for biomedical applications such as postoperative cavity filling and local drug delivery.

Keywords: gelatin; poly(*N*-isopropylacrylamide); photopolymerization; thermoresponsive hydrogels; injectable hydrogels; drug delivery systems

Academic Editor: Giuseppe Cavallaro

Received: 13 April 2026
Revised: 6 May 2026
Accepted: 22 May 2026
Published: 26 May 2026

1. Introduction

In the last decade, there has been a growing interest in injectable hydrogels as regenerative materials with therapeutic agents due to their ability to be universally administered into cavities of any shape. One type of such hydrogels includes systems based on a thermosensitive gelation mechanism [1,2]. The principle of action of thermosensitive injectable hydrogels is based on the reversible sol–gel transition of the polymer upon temperature change [3]. At room temperature, such compositions remain liquid or soft gel, allowing

for easy injection through a thin needle into hard-to-reach areas of the body [4]. However, upon contact with body tissues, they solidify, forming a stable three-dimensional network. This unique feature makes them ideal candidates for minimally invasive medicine, as they enable the local delivery of drugs or cells, filling tissue defects of any shape without the need for surgical intervention or subsequent removal of the carrier.

The combination of polymers with lower (LCST) and upper (UCST) critical solution temperatures within a single material offers unique opportunities for the fabrication of intelligent biomedical materials with programmable temperature responsiveness [5–7]. Such systems are capable of undergoing sol–gel transitions within a narrow temperature window. To date, a number of polymers are known to exhibit thermoresponsive behavior with LCST in aqueous environments. Among them are poly(ethylene oxide)-*b*-poly(propylene oxide)-*b*-poly(ethylene oxide) (PEO-*b*-PPO-*b*-PEO, also known as Pluronic or Poloxamer) [8], poly(*N*-vinylcaprolactam) (PNVCL) [9], poly(oligo(ethylene glycol) methacrylates) (POEGMAs) [10], polyoxazalines (POx) [11], poly(*N*-isopropylacrylamide) (PNIPAM) [12], poly(lactide-*co*-glycolide)-*b*-poly(ethylene glycol)-*b*-poly(lactide-*co*-glycolide) (PLGA-*b*-PEG-*b*-PLGA) [13,14], etc., as well as biodegradable polypeptides [15,16] and polypeptoids [17]. Examples of polymers exhibiting UCST behavior include well-known natural polymers [18], such as gelatin, carrageenan, and agarose, as well as synthetic polymers, including poly(3-dimethyl(acryloyloxyethyl)ammonium propanesulfonate) [19], poly(sulfobetaine methacrylate) [20], poly(methacrylamide) [21], poly(allylamine-*co*-allylurea) [22], poly(*N*-acryloylglycinamide) [23], etc.

Among the polymers characterized by LCSTs, PNIPAM offers a range of distinct advantages. Specifically, PNIPAM is one of the most studied polymers exhibiting an LCST in aqueous media. It is completely soluble in water at low temperatures but undergoes a phase transition and precipitates when heated above the LCST (around 32–34 °C) [24]. This falls between room temperature (20 °C) and body temperature (37 °C), making PNIPAM ideal for biomedical use. This behavior is a direct consequence of the polymer's amphiphilic nature, as each repeating unit features both hydrophilic and hydrophobic groups [25]. Below the LCST, PNIPAM chains remain hydrated and soluble due to hydrogen bonding between water and the polymer's C=O and N-H groups. Above the LCST, these intermolecular bonds become entropically unfavorable. Thermal motion disrupts the ordered hydration shells surrounding the hydrophobic isopropyl fragments, prompting the polymer chains to minimize contact with water. Hydrogen bonds with the solvent are broken, while intra- and intermolecular interactions among polymer segments become dominant. This leads to a sharp coil-to-globule transition, followed by chain aggregation and macroscopic phase separation. For temperature-responsive hydrogels, this transition is termed the volume phase transition temperature (VPTT) [26]. Below the VPTT, the gel is swollen, transparent, and soft. Above the VPTT, the gel collapses (shrinks), expels water, and sharply decreases in volume, becoming opaque (cloudy or white) and more rigid. The VPTT is often slightly higher than the LCST of linear PNIPAM due to elastic retractive forces within the network that resist collapse.

Moreover, in contrast to other thermosensitive polymers, PNIPAM exhibits an extremely sharp, cooperative hydrophilic-to-hydrophobic transition within a 1–2 °C window. This behavior is independent of its molecular weight, unlike, for example, polymers such as PNVCL [27]. In addition, the LCST of PNIPAM is easily tunable via copolymerization [28,29] or grafting to natural polymers [30,31]. Incorporating hydrophilic monomers (e.g., acrylamide) raises the LCST, while hydrophobic monomers (e.g., butyl methacrylate) lower it. Furthermore, the phase transition is also influenced by environmental factors such as ionic strength and the presence of organic solvents or other polymers. The LCST of copolymers containing ionizable groups is shifted by a change in the pH of the medium

and decreases as the system approaches the isoelectric point [31,32]. An increase in ionic strength or the addition [33,34] of organic solvents [35] also contributes to a decrease in the LCST value.

The main limitation of PNIPAM-based materials is that PNIPAM has not yet been approved by the Food and Drug Administration (FDA) agency for wide clinical use and remains an experimental polymer with "for research use only" status. The non-biodegradable nature of the main polymer chain (a carbon–chain polymer) imposes restrictions on the molecular weight of PNIPAM for the development of biomedical materials. Nevertheless, the development of toxicological research protocols for PNIPAM-containing nanomaterials brings PNIPAM closer to clinical trials [36]. However, for biomedical applications, complete removal of the monomer after synthesis is mandatory due to its known toxicity [37].

Of the UCST polymers used in the fabrication of biomedical materials for in vivo applications, collagen-derived gelatin (GN) is of considerable interest due to its exceptional biocompatibility, low immunogenicity, and biodegradability [38]. Due to the presence of cell-adhesive sequences (RGD) in its structure [39], gelatin and its derivatives are widely used to fabricate tissue engineering scaffolds, controlled drug delivery systems, and wound dressings, providing an optimal environment for tissue regeneration and wound healing. Gelatin's key feature lies in its ability to transition from a sol to a gel state upon cooling (UCST ~ 25–35 °C). In this case, the polypeptide chains restore helical structures and form physical crosslinks through hydrogen bonds and hydrophobic interactions. As a result, below the UCST, aqueous gelatin solutions form thermoreversible physical hydrogels. Above the UCST, thermal motion disrupts these physical crosslinks, hydrophobic interactions weaken, and the gel melts, transitioning into a liquid sol.

The combination of GN and PNIPAM started from the investigation of the fundamental thermoresponsive behavior of their mixtures, demonstrating that PNIPAM, characterized by an LCST, and GN, characterized by a UCST, can be integrated to create reversible complexation and aggregation in solution [40]. Ohya et al. expanded this concept by developing covalently grafted copolymers. Using iniferter-mediated photopolymerization, they grew PNIPAM chains directly from a gelatin backbone, yielding materials capable of forming physical hydrogels at physiological temperature [41,42]. Boudet et al. introduced an alternative strategy utilizing a thermosensitive PNIPAM-based copolymer as a reactive crosslinker for gelatin, enabling the formation of chemically crosslinked hydrogels [43]. Subsequently, Tsai et al. focused on creating composite interpenetrating polymer network (IPN) hydrogels consisting of a PNIPAM hydrogel crosslinked with *N*,*N*-methylene bisacrylamide (MBA) filled with gelatin and polystyrene nanoparticles as pore-forming templates. This approach yielded hydrogels with thermo-tunable pore sizes, enabling precise "smart gating" for controlled drug release, where the pore opening and closing are governed by the coil-to-globule transition of PNIPAM and the swelling behavior of gelatin [44]. Recently, Parvathy et al. reported the preparation of GN/PNIPAM nanogels crosslinked via gelatin's amine groups using terephthaldehyde-based nanoparticles. The resulting nanogels exhibited a combination of advantageous properties, including injectability, self-healing behavior, fluorescence, and thermoresponsiveness [45]. Other recent studies have employed IPN hydrogels for drug delivery applications. For instance, Lee et al. impregnated PNIPAM into a GN network to create an IPN hydrogel for local drug delivery [46]. In a separate approach, Daaboul et al. developed poly(lactide-co-glycolide) nanoparticles embedded into P(NIPAM-*co*-poly(ethylene glycol) diacrylate)/GN IPN hydrogels to achieve sustained drug release from the composite hydrogel [47].

In contrast to previously reported studies, this work presents the synthesis of GN-PNIPAM microgels via rapid UV-mediated photopolymerization of methacrylated GN (GN-MA) and NIPAM. Subsequent freeze-drying of the microgels, followed by rehydrating

of the dried gel, yielded a soft, injectable hydrogel that stiffens above the LCST of PNIPAM. Additionally, a series of crosslinked hydrogels was prepared by varying the amounts of the crosslinking agent (MBA) added into the polymerization mixture. The polymerization process was modulated by altering the component ratios, UV irradiation time, and crosslinker concentration.

2. Materials and Methods

2.1. Materials and Supplements

Food grade gelatin (Type B) (M_n = 33,000 Da, $Đ$ = 1.83) was purchased from Bargus Trade (St. Petersburg, Russia). Reagents for modification and polymerization, namely, methacrylic anhydride (MAA, ≥98%), NIPAM (99%), MBA (≥99.5%), and 2-hydroxy-2-methylpropiophenone (Darocur 1173, 97%), were purchased from Sigma-Aldrich (Darmstadt, Germany). Moxifloxacin hydrochloride (MOX, ≥98%) was also purchased from Sigma-Aldrich (Darmstadt, Germany). Sodium hydroxide (NaOH, >99%) and hydrochloric acid (HCl, 37%) were purchased from Vekton (St. Petersburg, Russia) and used to prepare solutions in deionized water. A 0.1 M PBS solution was supplied by Eco-Service (St. Petersburg, Russia) and diluted tenfold with deionized water before use.

Dialysis membrane bags (MWCO 2000 Da and 14,000 Da) and SpectraPor Biotech tubes (MWCO 3500 Da) were purchased from Repligen Corp. (Boston, MA, USA).

Human skin fibroblasts (DF2 cell line) used for in vitro biological evaluation were derived from the Cell Collection of the Institute of Cytology of the Russian Academy of Sciences (St. Petersburg, Russia). DMEM/F12 culture medium (Dulbecco's Modified Eagle's Medium) (Biolot, Saint-Petersburg, Russia), supplemented with 10% (*v*/*v*) heat-inactivated fetal bovine serum (FBS; HyClone, Logan, UT, USA), 1% L-glutamine, 50 U/mL penicillin, and 50 μg/mL streptomycin, was purchased from Biolot (St. Petersburg, Russia).

2.2. Synthesis and Characterization of GN-MA

The synthesis of GN-MA was carried out as follows. In a glass reaction vessel, 10 g of gelatin was dissolved in 100 mL of 0.1 M carbonate–bicarbonate buffer solution (pH 9) at a temperature of 60 °C with vigorous stirring (800 rpm) until complete dissolution was achieved (~60 min). The resulting solution was cooled to 50 °C under continuous stirring. After 30 min, methacrylic anhydride (MAA, 250 μL) was added. The methacrylation reaction was then conducted for 60 min at 50 °C with a stirring speed of 500 rpm. To maintain the pH of the reaction mixture at 9, a 0.01 M NaOH solution was added periodically. The reaction was quenched by reducing the pH to 7.0 by 6 M HCl solution.

The resulting GN-MA solution was purified from unreacted reagents and by-products by dialysis against a large volume of deionized water at 40 °C for 48 h. During dialysis, the water was replaced every 4 h in the daytime, resulting in 3–4 total water changes per 24 h under constant stirring; dialysis membrane bags with a MWCO of 14,000 Da were used. After dialysis was complete, the GN-MA solution was subjected to freeze-drying using a Labconco FreeZone freeze-dryer (Kansas, MO, USA) to obtain a solid powder. The final product was stored in the dark at −20 °C to prevent degradation and unwanted polymerization until further use.

To confirm the chemical modification of GN with PNIPAM, attenuated total reflectance Fourier transform infrared (ATR-FTIR) spectroscopy was used. GN-MA samples were prepared for analysis as thin films using a solution casting technique and subsequently dried in air. FTIR spectra were recorded on an IRAffinity-1 S spectrometer (Shimadzu, Tokyo, Japan) in transmission mode over the wavenumber range from 1000 to 3500 cm^{-1}, with a resolution of 2 cm^{-1} and 40 scans per sample. Deconvolution of FTIR spectra was performed using Origin Pro 8.6 software (OriginLab, Northampton, MA, USA). Normaliza-

tion of peak areas was performed by calculating the ratio of the peak area of the band of interest to the sum of the bands of GN at 1644 and 1655 cm^{-1}, which correspond to Amide I in α-helices and random coils of GN.

For the quantitative determination of the degree of methacrylation, proton nuclear magnetic resonance (^{1}H NMR) spectroscopy of a 400 MHz operation frequency was used. Samples of lyophilized GN-MA were dissolved in D_2O. NMR spectra were recorded using an Avance AV-400 spectrometer (Bruker, Karlsruhe, Germany) at 25 °C. The degree of modification was calculated from the obtained ^{1}H NMR spectra. Since the signal of the aromatic amino acid protons (7.24 ppm) in GN remains constant, its intensity was used to normalize the intensity of other protons in different samples. The degree of substitution (%) was calculated as described elsewhere [48].

2.3. Synthesis and Characterization of GN-PNIPAM Microgels

In separate glasses, GN-MA, NIPAM and Darocur 1173 stock solutions in deionized water were prepared. Polymerization mixtures were then prepared in separate vials by mixing certain proportions of the solutions of GN-MA, NIPAM, and Darocur 1173, which served as a Type I photoinitiator. For a portion of the samples, the crosslinking agent MBA was additionally introduced under variation in its molar concentration relative to the total amount of monomers. The composition of the polymerization mixtures used is shown in Table 1. Photocopolymerization of GN-MA with NIPAM results in the formation of GN-containing grafted PNIPAM chains with possible self-crosslinking, denoted in this work as GN-PNIPAM. Photocopolymerization of GN-MA with NIPAM in the presence of MBA leads to the formation of crosslinked GN-PNIPAM network, denoted in this work as GN-PNIPAM-cl.

Table 1. Compositions of polymerization mixtures used for the synthesis of microgels.

Sample	Composition (wt%)			
	GN	**NIPAM**	**MBA**	**Darocur-1173**
GN-PNIPAM-1	1.0	1.0	0	0.5
GN-PNIPAM-1.5	1.5	1.5	0	0.5
GN-PNIPAM-1.5-cl1	1.5	1.5	0.025	0.5
GN-PNIPAM-1.5-cl2	1.5	1.5	0.05	0.5
GN-PNIPAM-1.5-cl3	1.5	1.5	0.20	0.5
GN-PNIPAM-1.5-cl4	1.5	1.5	0.50	0.5
GN-PNIPAM-1.5-cl5	1.5	1.5	0.80	0.5
GN-PNIPAM-1-3	1.0	3.0	0	0.5

The resulting homogeneous polymerization mixtures were purged with argon for 10 min, and 1.5 mL of the mixtures was poured into quartz cuvettes and subjected to photopolymerization via UVA irradiation (Fotolab UV Composite Photo Polymerization Oven, TISSIDental, Milan, Italy). Depending on the composition, the exposure time was varied between 90 and 480 s. Irradiation was provided by 9 lamps, including 8 PLS lamps of 9 W and a 150 W halogen lamp, resulting in a total power of 222 W.

After photopolymerization was complete, the obtained samples were carefully transferred to dialysis bags with a MWCO of 14,000 Da and purified against water for 48 h with multiple water changes to determine yield and obtain monomer-free samples for further characterization. The product yield was calculated as the ratio of the mass of the obtained purified and dried polymer product to the total mass of the components of the polymerization mixture, expressed as a percentage.

The hydrodynamic diameter (D_H) of the microgels was measured with a Zetasizer Nano-ZS Malvern Panalytical (Malvern, UK) equipped with a He-Ne laser (633 nm).

Measurements were performed in water at a concentration of 0.2 mg/mL at 25 or 40 °C and a scattering angle of 173°.

Enzymatic degradation of GN in GN-PNIPAM was performed with the use of papain. With this aim, GN-PNIPAM (10 mg/mL) was incubated with papain (1 mg/mL, pre-dissolved in 0.1 M acetate buffer, pH 5.5) for 24 h at 37 °C. After incubation, the reaction mixture was centrifuged in dialysis tubes (MWCO 15,000 Da), and the filtrate was subjected to lyophilization for further size exclusion chromatography (SEC). The latter was performed using a Shimadzu LC-10 chromatographic system (Kyoto, Japan). The separation was carried out using a PLgel Guard pre-column (5 µm, 50 × 7.5 mm) and two PLgel MIXED-D columns (5 µm, 7.5 × 300 mm) from Agilent Technologies (Santa Clara, CA, USA). THF was used as the mobile phase. The analyses were performed at 40 °C with a flow rate of 1 mL/min. The molecular weight characteristics were determined using Shimadzu LC Solution 1.24SP1 GPC software (Kyoto, Japan). The molecular weights were calculated relative to a calibration plot built with polystyrene standards.

2.4. Preparation and Characterization of GN-PNIPAM Hydrogel

The bulk hydrogel was prepared by freeze-drying the GN-PNIPAM microgel water dispersion, allowing the particles to assemble into a continuous structure with interconnected pores [49]. Dry sponge-like continuous polymer matrices were placed in water to obtain hydrogels.

The quantity of bound water in the GN-PNIPAM hydrogels was investigated by differential scanning calorimetry (DSC) using a DSC-60 Shimadzu instrument (Shimadzu, Kyoto, Japan). For analysis, 10–15 mg samples of the hydrogel pre-swollen to equilibrium were placed in sealed aluminum pans. Measurements were performed over a temperature range from −50 °C to 200 °C at a heating rate of 10 °C/min. Data were recorded and analyzed using ta60 software, version 2.21.

The rheological properties of the GN-PNIPAM hydrogels were investigated to determine their mechanical characteristics and temperature sensitivity. Measurements were performed using a rotational MCR302 Anton-Paar rheometer (Graz, Austria). Before measurements, the samples were swollen to equilibrium. The following types of measurements were performed. Amplitude oscillatory sweep: measurement of G′ and G″ with increasing amplitude (at 10 rad/s, 20 °C and 40 °C) to determine the linear viscoelastic (LVE) region and gel strength. Frequency sweep: measurement of G′ and G″ as a function of frequency (at 20 °C and 40 °C) to evaluate viscoelastic behavior. Data were processed using RHEOPLUS/32 V.3.62 software.

The surface morphology of dry hydrogels was evaluated using a Hitachi S-3400N (Tokyo, Japan) scanning electron microscope (SEM).

The swelling of hydrogels was studied in 0.01 M PBS (pH 7.4) over time. The maximal swelling (Q_{max}) was calculated as the ratio of the difference between the mass of the swollen sample and the mass of the dried sample to the mass of the dried sample. To describe the diffusion of the solvent into the hydrogel, the pseudo-first-order and pseudo-second-order models, as well as the Peleg and Peppas models, were used [50,51].

2.5. MOX Loading to GN-PNIPAM Hydrogel and Release Study

MOX was dissolved in distilled water at a concentration of 10 wt% relative to the weight of the polymer matrix. The freeze-dried GN-PNIPAM was immersed in the MOX solution to load the drug substance via passive diffusion and matrix swelling [52,53].

The release study was conducted using a dialysis method. Samples in 0.01 M PBS (pH 7.4) were incubated in 1 mL dialysis tubes with a MWCO of 3500 Da over time at 37 °C. At predetermined time intervals, 0.5 mL aliquots were withdrawn from the 10 mL

outer chamber filled with 0.01 M PBS (pH 7.4). The amount of released substance in solution was determined spectrophotometrically at a wavelength of 288 nm (LOMO SF-56, St. Petersburg, Russia). For quantification, the calibration plot previously built for standard MOX solutions was used. The fraction of antibiotic released from the hydrogel was calculated as the percentage ratio of the mass of free antibiotic at time t to the mass of antibiotic loaded into the hydrogel. The percentage of antibiotic released from the hydrogel at a given time (t) was determined by dividing the mass of free antibiotic at time t by the mass of antibiotic initially loaded into the hydrogel. For the evaluation of the MOX release mechanism from the hydrogel matrix, the Higuchi, Korsmeyer–Peppas, and pseudo-first-order models were applied [54,55].

2.6. In Vitro Biological Evaluation

DF2 cells were cultured in a CO_2 incubator at 37 °C in a humidified atmosphere containing air and 5% CO_2 in DMEM/F12 medium.

To evaluate the cytotoxicity of the GN-MA and GN-PNIPAM microgels, 5×10^3 cells/100 μL/well were seeded into 96-well plates and cultured for 12 h for their attachment. After that, the medium was removed, and a medium containing the testing samples at concentrations ranging from 4 to 1000 μg/mL was added to the wells with attached cells. At the end of the incubation period (72 h), the medium was removed, and 50 μL/well of DMEM/F12 medium with MTT reagent (0.1 mg/mL) was added. The cells were incubated in a CO_2 incubator for 2 h at 37 °C. After removing the supernatant, the formazan crystals formed by metabolically viable cells were dissolved in DMSO (50 μL/well) and transferred to clean wells for spectrophotometric analysis. Optical density was measured at 570 nm using a plate reader. The data were processed using Excel software (MS Office 2019, Redmond, WA, USA).

To evaluate the adhesion of the cells on the surface of the GN-PNIPAM hydrogels, initially, 150 μL of GN-PNIPAM was injected into the wells of the 96-well plates and pre-incubated for 30 min at 37 °C for gelation. After that, 5×10^3 cells/100 μL of DMEN/F12 were seeded on the surface of the hydrogel samples and empty wells for the control. The cells were cultured for 72 h. The subsequent steps were identical to those described for the cytotoxicity study of the microgels.

2.7. Statistics

All synthetic procedures were repeated 3–5 times for the same composition. Rheological experiments were performed in triplicate for samples of each composition from different batches, and the data were averaged. Biological experiments were repeated 4 times for microgels and 3 times for hydrogels. The data are presented as the mean ± standard deviation (SD) value.

3. Results and Discussion

3.1. Synthesis and Characterization of GN-PNIPAM Microgels

The synthesis of the GN-PNIPAM microgels is illustrated in Figure 1. The process involved two steps: (1) the methacrylation of GN's lysine groups with methacrylic anhydride to introduce vinyl functionality (Figure 1A) and (2) the photoinitiated copolymerization of PNIPAM with GN-MA to form the microgel dispersions (Figure 1B).

The methacrylation of GN was confirmed by ^{1}H NMR spectroscopy (Figure S1, Supplementary Materials). The appearance of new peaks corresponding to the protons of the methacryloyl group (vinyl protons at $\delta \approx 5.3$–5.8 ppm and methyl group protons at $\delta \approx 1.9$ ppm), along with the simultaneous decrease in intensity of the peak for the methylene protons adjacent to the ε-amino group of lysine residues ($\delta \approx 2.9$ ppm), confirmed

successful modification. The degree of modification calculated from the ^{1}H NMR spectra was 30 ± 2 mol%.

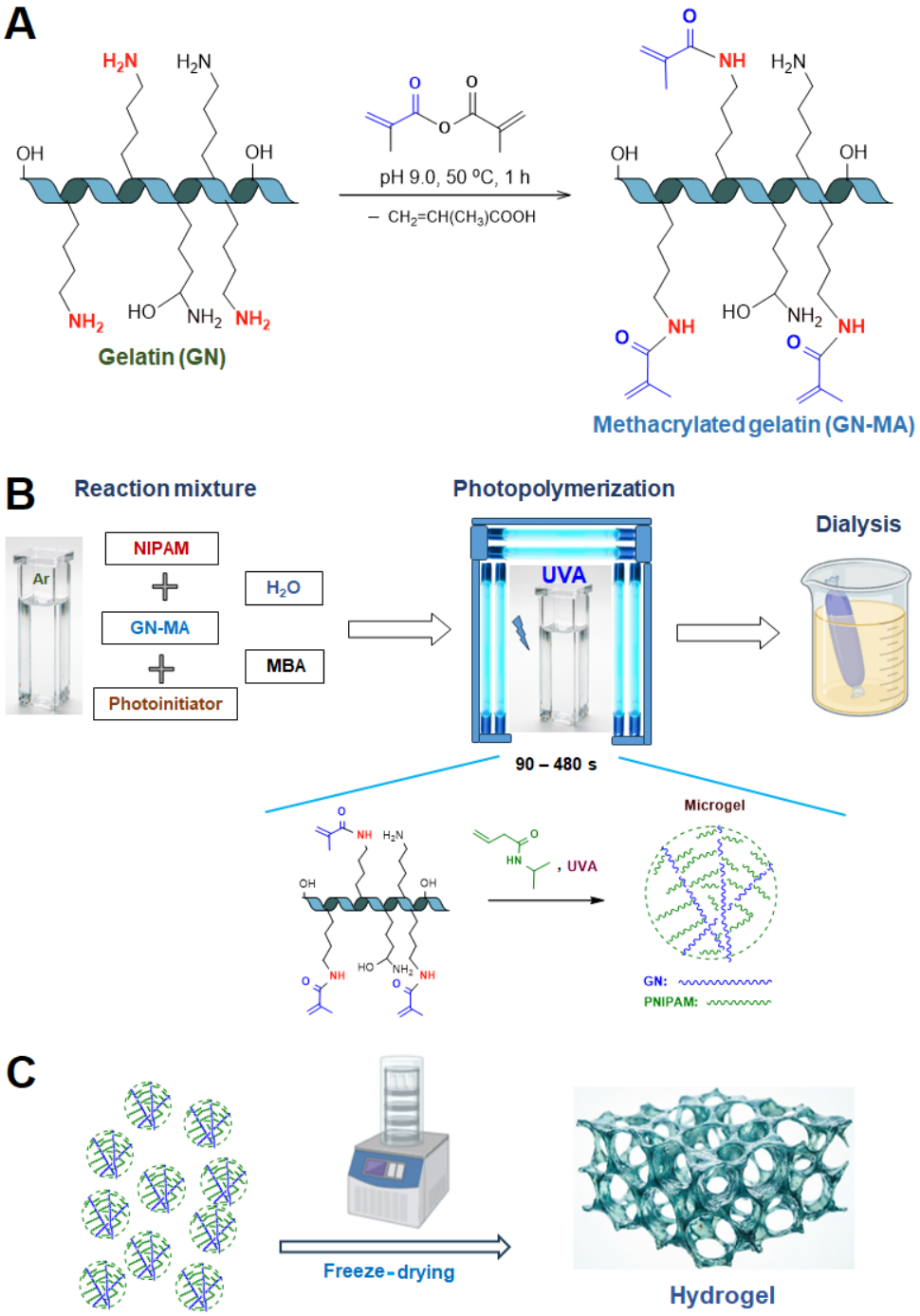

Figure 1. Scheme for microgel synthesis and hydrogel production: (**A**) gelatin methacrylation; (**B**) microgel synthesis from methacrylated gelatin and NIPAM via photopolymerization; (**C**) hydrogel production from microgel dispersion by freeze drying.

The product yield serves as a critical parameter for evaluating the efficiency of synthesis, directly reflecting the conversion of monomer to polymer and the formation of the network structure [56,57]. In this context, to determine the optimal polymerization time that ensures a high yield of the polymer product, the dependencies of the product yield on the photopolymerization time were obtained (Figure 2). Upon UV irradiation of a reaction medium containing GN-MA, NIPAM, and a Type I photoinitiator (Darocure-1173),

several parallel processes can occur: (1) grafting of NIPAM onto GN-MA, (2) crosslinking of GN-MA chains, (3) homopolymerization of NIPAM in solution, and (4) recombination of free macroradicals. The probability of the last process is lower than that of the first three. The extent of the first three processes will significantly depend on the NIPAM concentration and the irradiation time. At low NIPAM concentrations, besides PNIPAM grafting, the competing crosslinking reaction between different GN chains is highly probable. As a result, a microgel composed of crosslinked GN-graft-PNIPAM chains is formed. The probability of homopolymerization as a side reaction will be significantly lower than that of the first two processes. Increasing the irradiation time will lead to an increase in the degree of crosslinking as well as the product yield due to monomer conversion into PNIPAM. At higher NIPAM concentrations, the radicals on GN-MA encounter NIPAM molecules more frequently, leading to an increase in the number of grafted chains as well as an increase in the probability of the competing process of homopolymerization in solution. The macroradical may still attack another GN-MA molecule (crosslinking). However, a large number of growing PNIPAM chains will further protect it and reduce the probability of this process.

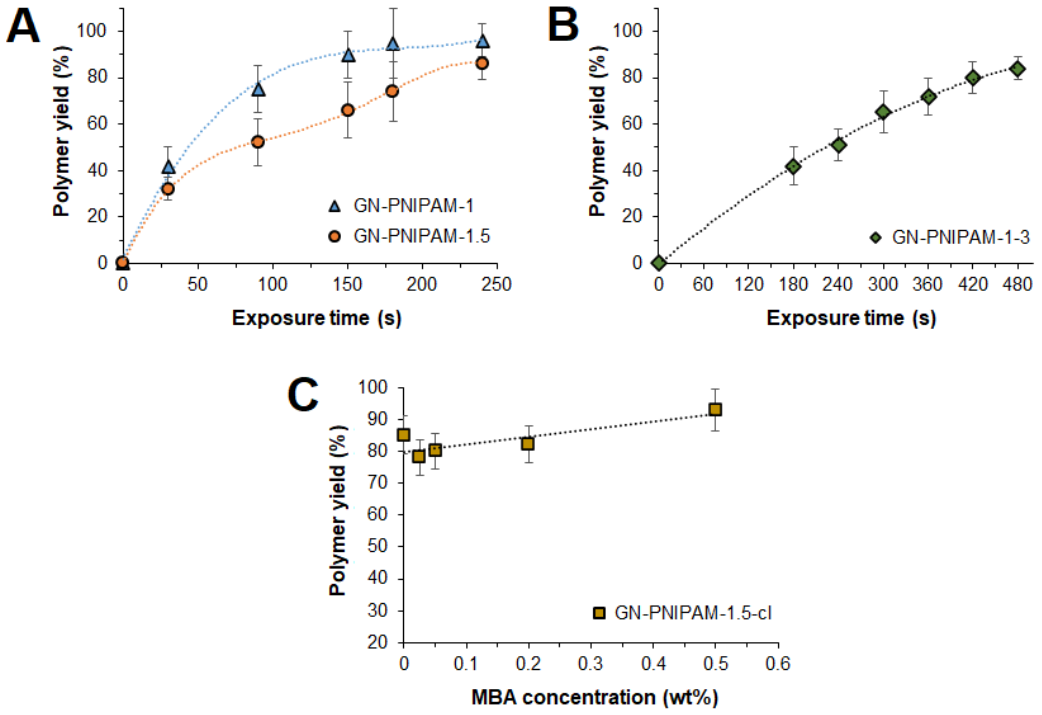

Figure 2. Dependence of GN-PNIPAM yield on exposure time (**A**,**B**) and MBA concentration (240 s) (**C**). Sample abbreviations corresponding to the polymerization mixture compositions are given in Table 1.

Analysis of the data (Figure 2) demonstrates significant variability in polymer yield depending on the initial reaction mixture composition. As expected, for GN-PNIPAM-1, the polymer yield was observed to increase rapidly, exceeding 90% within 180 s of UV irradiation (Figure 2A). A 1.5-fold increase in the concentrations of both GN-MA and NIPAM required longer polymerization times (240 s) to achieve a product yield of approximately 90% (Figure 2A). In turn, increasing the NIPAM concentration to 3 wt% while maintaining the GN-MA concentration at 1 wt% (GN-PNIPAM-1-3) required significant polymerization times ($\geq$420 s) to achieve a yield of $\geq$80% (Figure 2B). The decrease in product yield with increasing NIPAM content in the reaction medium may be a consequence of the formation of free PNIPAM due to both homopolymerization and the increased probability of chain termination on PNIPAM macroradicals. In turn, free PNIPAM is

removed during the purification step, reducing the yield of GN-PNIPAM microgel, which is further indirectly confirmed for polymerization in the presence of MBA.

In addition, a series of GN-PNIPAM microgels crosslinked with MBA was synthesized (GN-PNIPAM-1.5-cl). The effect of MBA content on PNIPAM microgel properties has been demonstrated in several studies. The authors have reported that increasing the crosslinker content leads to decreased microgel swelling and increased VPTT values [58–60]. An MBA content of up to 0.5 wt% is considered optimal to obtain microgels with good swelling and appropriate thermosensitivity. The crosslinker content may influence the thermoresponsive properties in different ways. Specifically, at too low crosslinker contents, the polymer chains are poorly connected. Although they could theoretically collapse, the network is too soft and loose to exert sufficient elastic cooperative force for efficient water expulsion. As a result, the collapse may be incomplete or non-uniform, or the hydrogel may undergo microphase separation without a dramatic macroscopic volume change. In contrast, at too high crosslinker contents, the network becomes overly rigid and dense. The polymer chains are so tightly constrained that they cannot rearrange or collapse significantly, even above the VPTT.

To determine the optimum crosslinker content for the GN-PNIPAM system, the MBA content was varied from 0.025 to 0.80 wt%, as this parameter can significantly influence the thermoresponsive properties. It was found that under otherwise identical conditions, increasing the crosslinker content leads to a higher product yield, which is attributed to the additional incorporation of growing PNIPAM chains into the gel network (Figure 2C).

Figure 3 shows the ATR-FTIR spectra of the polymerization mixture and purified and unpurified GN-PNIPAM synthesized at different exposure times. The FTIR spectrum of the reaction medium, composed of GN-MA and NIPAM, exhibits characteristic bands reflecting the composition of the mixture prior to polymerization. A broad O–H/N–H band is observed in the region of 3300–3500 cm^{-1}, belonging to both GN and NIPAM. In the 1630–1660 cm^{-1} range, the Amide I (C=O) band appears, along with Amide II (N–H) absorption bands at 1530–1550 cm^{-1}. A clear band at 3073 cm^{-1} in the spectrum of the reaction mixture corresponds to the stretching vibrations of =C–H (the double bond of the vinyl group of the NIPAM monomer). For single C–H bonds, bands in the range of 2850–2960 cm^{-1} are characteristic of $\delta_{as}(CH_3)$ ~2960 cm^{-1} and $\delta_s(CH_3)$ ~2870 cm^{-1}, which are typical for the methyl groups of NIPAM. The group of bands at 2972, 2930, and 2872 cm^{-1} corresponds to the stretching vibrations of aliphatic C–H bonds (methyl and methylene groups) in NIPAM and the methacrylic acid fragment in GN-MA. The weak intensity of the band at 3073 cm^{-1} in the spectra of the final GN-PNIPAM indicates that the polymerization was successful and the double bonds of the monomer were consumed. The characteristic bands of Amide I and Amide II at 1630–1660 cm^{-1} and 1530–1550 cm^{-1} remain pronounced, but their shape and relative intensity change. The bands at 1365 and 1387 cm^{-1} are characteristic of the isopropyl group present in PNIPAM, which confirms the polymer structure.

After washing the hydrogel, the spectra remain similar to those of the copolymer after synthesis. However, an additional decrease in the intensity of the band at 3290 cm^{-1} is observed, indicating the removal of residual low-molecular-weight impurities not incorporated into the network, along with a reduction in the monomer double bond band at 3073 cm^{-1}. The characteristic amide bands (1636, 1534 cm^{-1}) and the isopropyl group bands (doublet at ~1385 and ~1365 cm^{-1}) remain preserved.

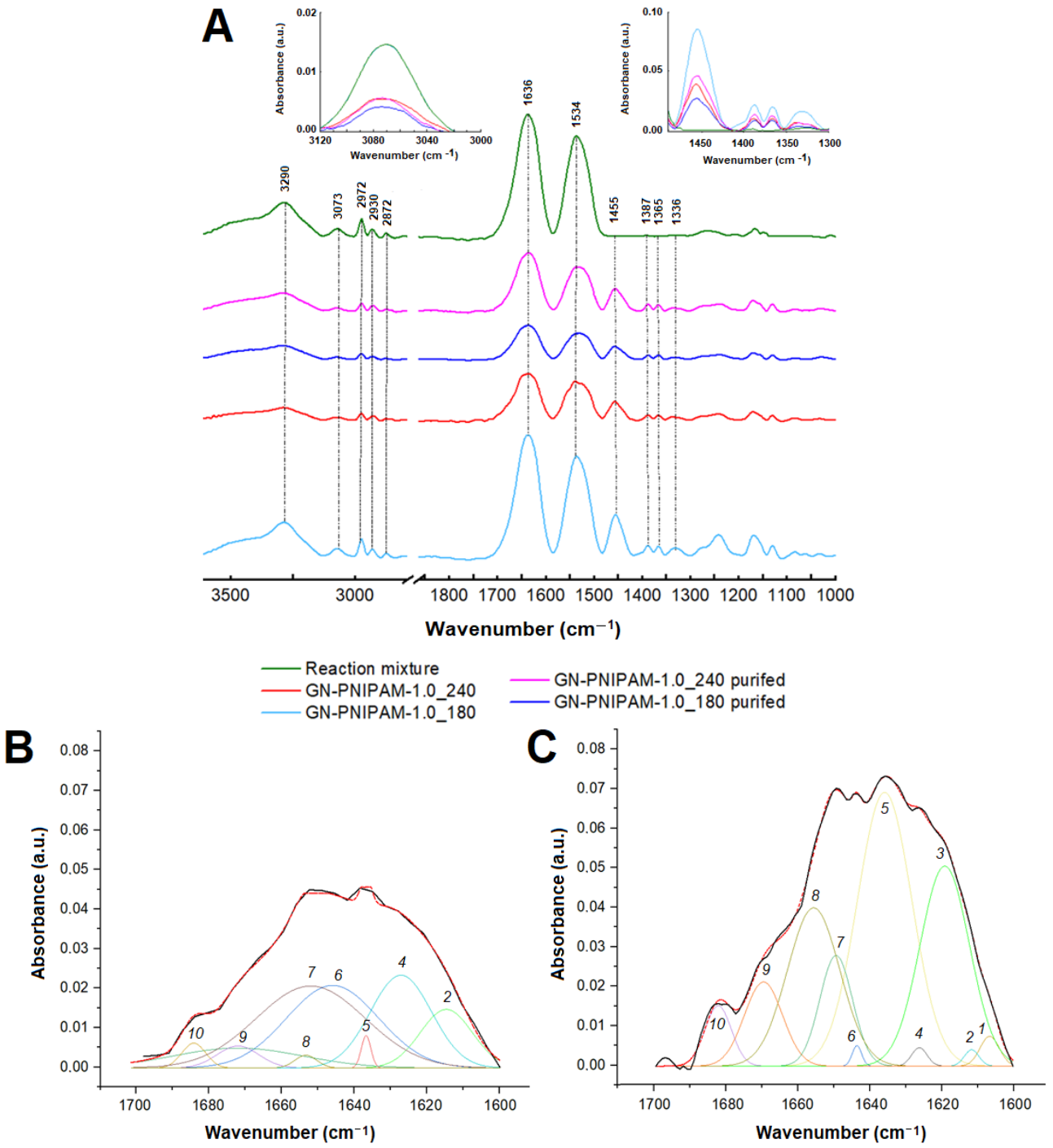

Figure 3. FTIR spectra of reaction mixture (GN-MA + NIPAM) and GN-PNIPAM-1 after synthesis and after purification (**A**) and fragment of FTIR spectra after deconvolution (Gaussian peak approximation) of reaction mixture (GN-MA + NIPAM) (**B**) and GN-PNIPAM-1 after polymerization within 240 s (**C**) in the region of 1600–1700 cm^{-1}. Bands in (**B**,**C**): 1—1607 cm^{-1}; 2—1613 cm^{-1}; 3—1620 cm^{-1}, 4—1627 cm^{-1}; 5—1636 cm^{-1}; 6—1644 cm^{-1}; 7—1651 cm^{-1}; 8—1655 cm^{-1}; 9—1671 cm^{-1}; 10—1683 cm^{-1}. The black solid line shows a fragment of the FTIR spectrum, while the red dashed line indicates the resulting approximation curve. Sample abbreviations corresponding to the polymerization mixture compositions are given in Table 1.

The deconvolution of FTIR spectra in the 1600–1700 cm^{-1} region revealed further pronounced changes when comparing the reaction mixture (GN-MA + NIPAM) with GN-PNIPAM-1 synthesized via UV irradiation within 240 s. Specifically, the peak at 1612 cm^{-1}, characteristic of the C=C stretching vibration (conjugated with C=O), as well as the Amide I

band of free or weakly bound amides at 1650 cm^{-1}, decreased drastically in the spectrum of GN-PNIPAM-1 (normalized peak area: 0.03 at 1612 cm^{-1} and 1.14 at 1650 cm^{-1}) compared to the spectrum of the reaction mixture (normalized peak area: 0.03 at 1612 cm^{-1} and 1.14 at 1650 cm^{-1}). This testifies to the depletion of double bonds and free monomer during polymerization. At the same time, the Amide I band corresponding to the disordered structure (random coil) at 1636 cm^{-1}, characteristic of PNIPAM, increased significantly for GN-PNIPAM-1 (normalized peak area = 1.75) compared to the same band detected in the reaction mixture (normalized peak area = 0.04).

The length of the grafted PNIPAM chains was evaluated by SEC analysis of the samples subjected to enzymatic hydrolysis of GN in GN-PNIPAM. To this end, papain, a protease with broad substrate specificity, was employed as the biocatalyst. The hydrolyzed samples were subjected to the extraction of PNIPAM with THF and analyzed by SEC in THF (Table 2). The data indicate that when the NIPAM content in the reaction mixture was 1.0 wt%, PNIPAM chains with lengths close to the theoretically expected values (calculated regarding the content of methacrylate groups in GN-MA) were grafted. Increasing the monomer content simultaneously with GN-MA to 1.5 wt% led to the grafting of the longer PNIPAM chains. This fact can be explained by a combination of kinetic effects. In particular, an increase in monomer concentration directly accelerates the chain propagation rate, while an increase in the overall viscosity of the reaction medium upon raising the GN-MA concentration to 1.5 wt% and NIPAM to 1.5 wt% provides the increase in system viscosity. As a result, this diffusionally limits bimolecular radical termination but does not hinder the addition of small monomer molecules, which collectively favors the chain elongation.

Table 2. Comparison of theoretical and experimentally determined lengths of PNIPAM chains grafted to GN-MA. SEC analysis of PNIPAM extracted from enzymatic hydrolysates of GN-PNIPAM in THF (THF, 40 °C).

Conditions			Theoretically Expected Parameters		Experimentally Determined Characteristics		
GN-MA (wt%)	**NIPAM (wt%)**	**Exposure Time (s)**	***DP***	***M* ***	M_n	$Đ$	***DP***
1.0	1.0	180	10	1130	800	1.75	7
1.5	1.5	240	10	1130	1740	1.16	15
1.0	3.0	480	30	3390	1850	1.14	16

* Calculated without the contribution of initiator moieties.

Increasing the NIPAM concentration from 1.0 wt% to 3.0 wt% resulted in a chain length that was nearly twice as short as the theoretical value (*DP* = 16). This is attributed to the increase in the probability of the competing homopolymerization process in solution and the reduction in the part of NIPAM that participates in grafting. This is indirectly supported by a decrease in the yield of the target product compared to systems containing lower NIPAM concentrations.

The hydrodynamic diameters (D_H) of the GN-PNIPAM microgels were measured by DLS at temperatures below (20 °C) and above (40 °C) VPTT (Table 3). The DLS analysis at 20 °C showed that the PNIPAM microgels had D_H values ranging from 354 to 1022 nm, with the greatest size observed for the system additionally crosslinked with 0.2 wt% MBA. Upon heating to 40 °C, the microgels expectedly collapsed. For the GN-PNIPAM-1 and GN-PNIPAM-1.5 microgels, the hydrodynamic diameter decreased by a factor of 2.

In contrast, the most pronounced reduction in hydrodynamic diameter was observed for the GN-PNIPAM-1-3 microgels and the microgels obtained with additional crosslinking using MBA. In these cases, the particle size decreased by a factor of 4–5. This pronounced collapse reflects the superior swelling capacity of this system, attributed to its network retaining a larger amount of water. Thus, the introduction of MBA influenced the swelling

and hydrodynamic diameter of the microgels but retained the sharp thermosensitive response. Overall, the obtained data are in agreement with the known behavior of PNIPAM-containing microgels, which exhibit sizes ranging from 100 to 1000 nm and undergo a 3- to 6-fold reduction in diameter above the VPTT [61].

Table 3. Hydrodynamic diameters of microgels at temperatures below and above VPTT (DLS, H_2O).

Sample *	Polymerization Time (s)	D_H (nm)		α **
		20 °C	40 °C	
GN-PNIPAM-1	180	354 ± 20	183 ± 14	0.14
GN-PNIPAM-1	240	496 ± 29	308 ± 17	0.24
GN-PNIPAM-1.5	240	608 ± 64	305 ± 35	0.13
GN-PNIPAM-1-3	480	772 ± 35	176 ± 39	0.014
GN-PNIPAM-1.5-cl3	240	1022 ± 17	196 ± 57	0.007

* Sample abbreviations corresponding to the polymerization mixture compositions are given in Table 1. ** $\alpha = (D_{40}/D_{20})^3$.

One of the parameters characterizing the degree of compression is the ratio of the cubes of the microgel radii at temperatures above and below the phase transition temperature (α) [62]. This parameter indicates how many times the microgel volume decreases upon transitioning from the swollen state to the collapsed state. In the case of the GN-PNIPAM-1 and GN-PNIPAM-1.5 microgels, this parameter falls within the range of 0.13–0.24, reflecting moderate swelling and thermal sensitivity. In turn, the systems synthesized with increased NIPAM content (GN-PNIPAM-1-3) or with additional MBA crosslinking (GN-PNIPAM-1.5-cl3) exhibit a ratio of approximately 0.01, indicating pronounced swelling and thermal sensitivity.

In addition, the dynamics of the volume phase transition for the GN-PNIPAM-1-3 sample were monitored by DLS over the temperature range of 20–40 °C. As shown in Figure 4A, increasing the temperature from 20 to 30 °C had virtually no statistically significant effect on the hydrodynamic diameter of the microgels. A further temperature increase to 36 °C led to a sharp decrease in the hydrodynamic diameter, beyond which no significant changes were observed. Thus, the volume phase transition occurs within the range of 30 °C (T_1 or T_{onset}) to 36 °C (T_2 or T_{endset}). The VPTT value, determined from the differential plot shown in Figure 4B, was found to be 35 °C.

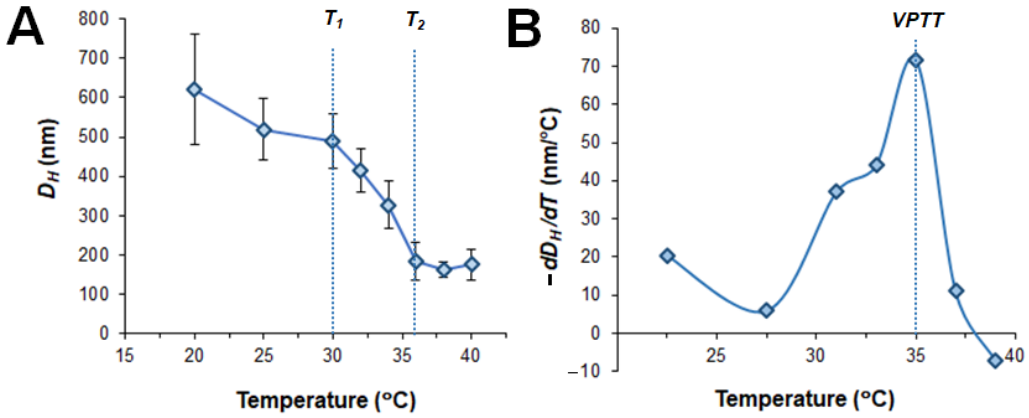

Figure 4. Dynamics of the microgel volume phase transition (DLS) as a function of temperature (**A**) and its differential plot (**B**) for the GN-PNIPAM-1-3 sample (see Table 1 for sample composition).

3.2. Preparation and Characterization of GN-PNIPAM Hydrogels

Microgel dispersions purified from monomer and free oligomers were lyophilized to yield porous sponge-like structures (Figure 1C) that can reswell in aqueous media and display thermosensitive behavior.

The surface morphology of the dry GN-PNIPAM hydrogel was analyzed by SEM (Figure 5). Freeze-drying of the microgel dispersion results in the formation of a sponge-like structure, characterized by a continuous polymer matrix penetrated by a network of interconnected macropores. The average pore size of the GN-PNIPAM hydrogel samples obtained was in the range of 50–90 µm.

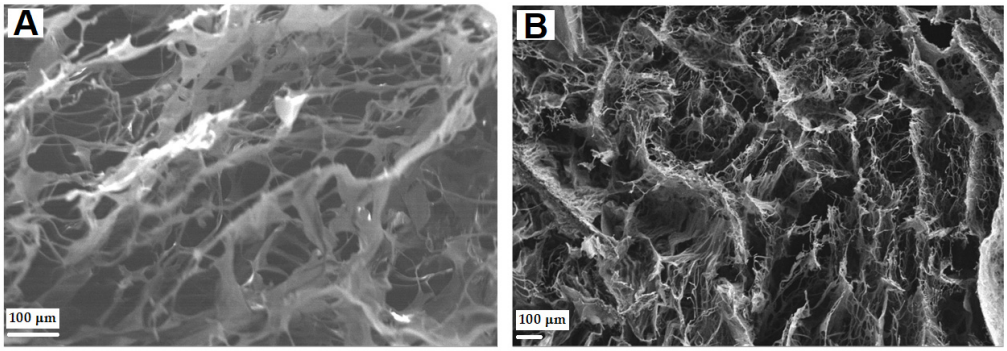

Figure 5. SEM images (200×) of dry bulk GN-PNIPAM hydrogels: (**A**) GN-PNIPAM-1.5-cl-4 (240 s) and (**B**) GN-PNIPAM-1-3 (480 s). Sample abbreviations corresponding to the polymerization mixture compositions are given in Table 1.

The ability of the dried hydrogel to swell over time in water at 20 °C and 40 °C was studied using GN-PNIPAM-1.5-cl5 as an example (Figure 6). Mathematical processing of the obtained swelling curves in water using pseudo-first-order and pseudo-second-order models, the Peleg model, and the Peppas model (Table 4) made it possible to evaluate the mechanism of water absorption during swelling under different temperature conditions. At 20 °C (<VPTT), a high equilibrium sorption capacity of Q_{max} = 46.8 g/g was achieved, characterized by anomalous diffusion (Peppas n = 0.78; Table 4) and following a pseudo-second-order kinetic model (k_2 = 0.178 $g^{-1} \cdot min^{-1}$, R^2 = 0.9999; Table 4). At 40 °C (>VPTT), a sharp collapse of the polymer network was observed, resulting in a significantly lower Q_{max} of 2.43 g/g. This marked difference in sorption capacity (from 46.8 to 2.43 g/g) is fully consistent with the thermosensitive behavior typical of PNIPAM-containing hydrogels. The high Q_{max} value of 46.8 g/g at 20 °C further indicates strong hydrophilicity, mainly related to GN presence.

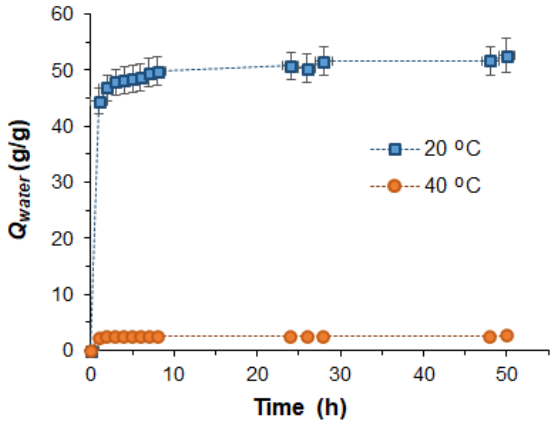

Figure 6. Water absorption by the dry GN-PNIPAM-1.5-cl5 hydrogel over time at 20 °C and 40 °C (see Table 1 for sample composition).

Table 4. Results of mathematical processing of water absorption plots using several standard models for the GN-PNIPAM-1.5-cl5 sample (see Table 1 for sample composition).

T (°C)	Pseudo-First-Order		Pseudo-Second-Order		Peleg Model			Peppas Model		
	K_1 (min^{-1})	R^2	K_2 ($g \cdot min^{-1}$)	R^2	K_1 ($g \cdot min^{-1}$)	K_2 (min^{-1})	R^2	n	K (min^{-1})	R^2
20	1.4×10^{-2}	0.9734	3.4×10^{-3}	0.9988	1.3	2×10^{-2}	0.9887	0.78	8.7×10^{-1}	0.9823
40	1.1×10^{-2}	0.9956	1.7×10^{-1}	0.9999	21.8	4×10^{-1}	0.9912	0.73	9.2×10^{-1}	0.9958

The best fit to the experimental data for both temperatures is provided by the pseudo-second-order model (R^2 = 0.99), as well as the Peleg and Peppas models. When the temperature changes from 20 °C to 40 °C, the sorption constants for the pseudo-second-order model (k_2) increase by more than 50 times. The exponent n in the Peppas model, ranging from 0.73 to 0.78, confirms the dominance of a diffusion process with a contribution from relaxation. The Peleg model demonstrates an acceleration of the initial swelling stage due to enhanced diffusive mobility of water molecules at an elevated temperature. Collectively, the data indicate thermosensitive behavior of the hydrogel with water sorption following a mixed mechanism, involving both diffusion through pores and relaxation of polymer chains, accompanied by significant structural rearrangement.

In PNIPAM-containing hydrogels, water serves not simply as a solvent but as a structural component that determines the phase behavior and properties of the material [63–65]. In particular, the amount of so-called bound water plays a crucial role, as it determines the energy required to initiate collapse. Bound water, with its high viscosity and low mobility, governs the injectability of hydrogels while preserving structural integrity. During collapse, the rate at which bound water is expelled determines the response rate of the material. A higher bound water content demands more energy for dehydration and can lead to an increase in the VPTT.

The bound water content of the GN-PNIPAM hydrogels was determined by DSC analysis [66]. On the thermograms obtained (Figure S2, Supplementary Materials), two endothermic peaks are observed. The first endothermic peak, recorded in the region around 0 °C, corresponds to the melting of ice formed from so-called "free" water that is not strongly bound to the polymer chains of the hydrogel. Its enthalpy allows the calculation of the fraction of free water. The second endothermic peak, which appears in the range of 90–105 °C, corresponds to the evaporation of both free and bound water. The difference between all evaporated water and free water corresponds to bound water. The latter is water that is tightly retained within the polymer matrix through hydrogen bonding and other strong interactions with the polymer chains, requiring significantly more energy for its removal than free water. According to the literature, the fraction of bound water in GN-based hydrogels (as determined by DSC analysis) is approximately 5–61%, depending on hydrogel concentration and composition [67–69].

Table 5 summarizes the DSC analysis data and the calculated contents of free and bound water in the GN-PNIPAM samples. As can be seen from the obtained data, the portion of bound water in the resulting GN-PNIPAM hydrogels ranges from 28 to 57% of the total water mass. With increasing GN concentration from 1.0 wt% to 1.5 wt%, the percentage of free water increased from 43–54% to 78–81% of the total water, while the fractions of bound water decreased. Moreover, longer irradiation times in the synthesis of GN-PNIPAM yield hydrogels with a lower bound water content. This may result from an increased grafting degree under longer irradiation, which generates more free radicals on the gelatin chains. This, in turn, enhances the overall hydrophobicity of the network, reducing the number of water molecules that can be strongly bound to the polymer matrix. Furthermore, irradiation induces both grafting and crosslinking (between gelatin chains and

between grafted PNIPAM chains), increasing crosslinking density, which limits hydrogel swelling and reduces bound water content [70]. The introduction of MBA as an additional crosslinking agent, as well as an increase in its content, favored the decrease in bound water content due to more extensive crosslinking of GN-PNIPAM chains.

Table 5. Determination of free and bound water content from DSC data.

Sample *	Polymerization Time (s)	H_m (J/g)	H_v (J/g)	$\varphi_{free\ water}$ (%)	$\varphi_{bound\ water}$ (%)
GN-PNIPAM-1	180	140	1040	43	57
GN-PNIPAM-1	300	174	1270	54	46
GN-PNIPAM-1.5	240	253	1990	78	22
GN-PNIPAM-1.5	300	175	1480	81	19
GN-PNIPAM-1-3	480	234	1900	72	28
GN-PNIPAM-1.5-cl4	240	180	1560	73	22
GN-PNIPAM-1.5-cl5	240	158	1270	84	16

* Sample abbreviations corresponding to the polymerization mixture compositions are given in Table 1.

Rheological studies allow detailed characterization of the viscoelastic properties and temperature response of hydrogels, along with quantitative evaluation of how composition affects their mechanical properties [71]. The rheological properties of the GN-PNIPAM hydrogels were investigated depending on hydrogel composition and synthesis time (Figure 7).

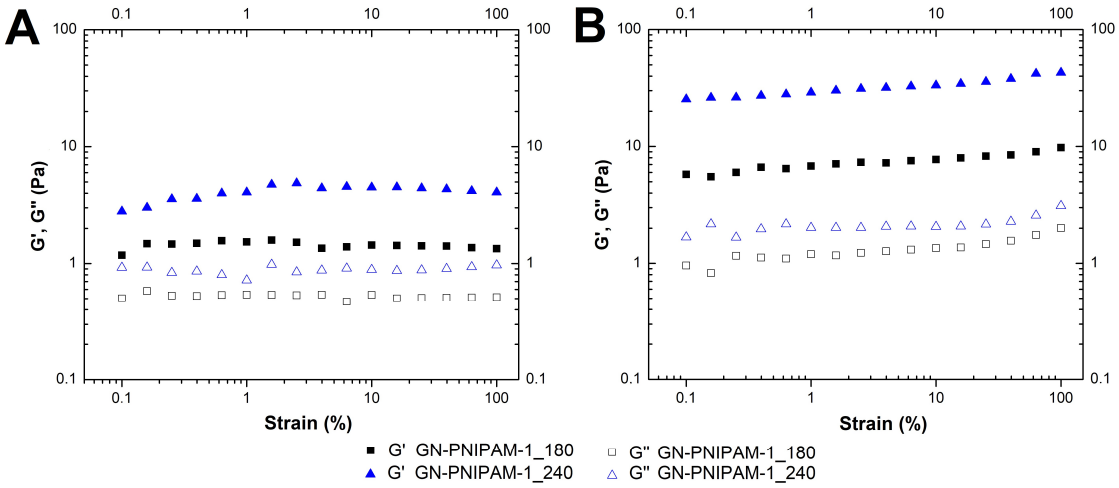

Figure 7. Sheer strain sweeps at the constant frequency of 10 rad/s measured at 20 °C (**A**) and 40 °C (**B**) for GN-PNIPAM-1 samples synthesized at different irradiation times (number at the end of sample code, s). Sample abbreviations corresponding to the polymerization mixture compositions are given in Table 1.

Oscillatory amplitude sweeps at 20 °C show that the samples exhibit linear viscoelastic behavior over the entire region (Figure 7A). Both the storage modulus (G′) and loss modulus (G″) demonstrated a linear trend up to 100% strain. At 40 °C, G′ showed a noticeable increase compared to 20 °C, reflecting the densification of the hydrogel network due to clustering of the PNIPAM hydrogels via hydrophobic interactions of the isopropyl groups of PNIPAM (Figure 7B). The 0.1–1.0% strain was selected for further frequency sweep studies.

In the frequency sweeps (frequency range 0.1–100 rad/s) at 20 °C for hydrogels GN-PNIPAM-1 (Figure 8A), GN-PNIPAM-1.5 (Figure 8C), as well as GN-PNIPAM-1.5-cl (Figure 8E), prepared with a low MBA content (0.025–0.50 wt%), the storage modulus G′ remained relatively stable in the low- and medium-frequency regions, while it increased at high frequencies.

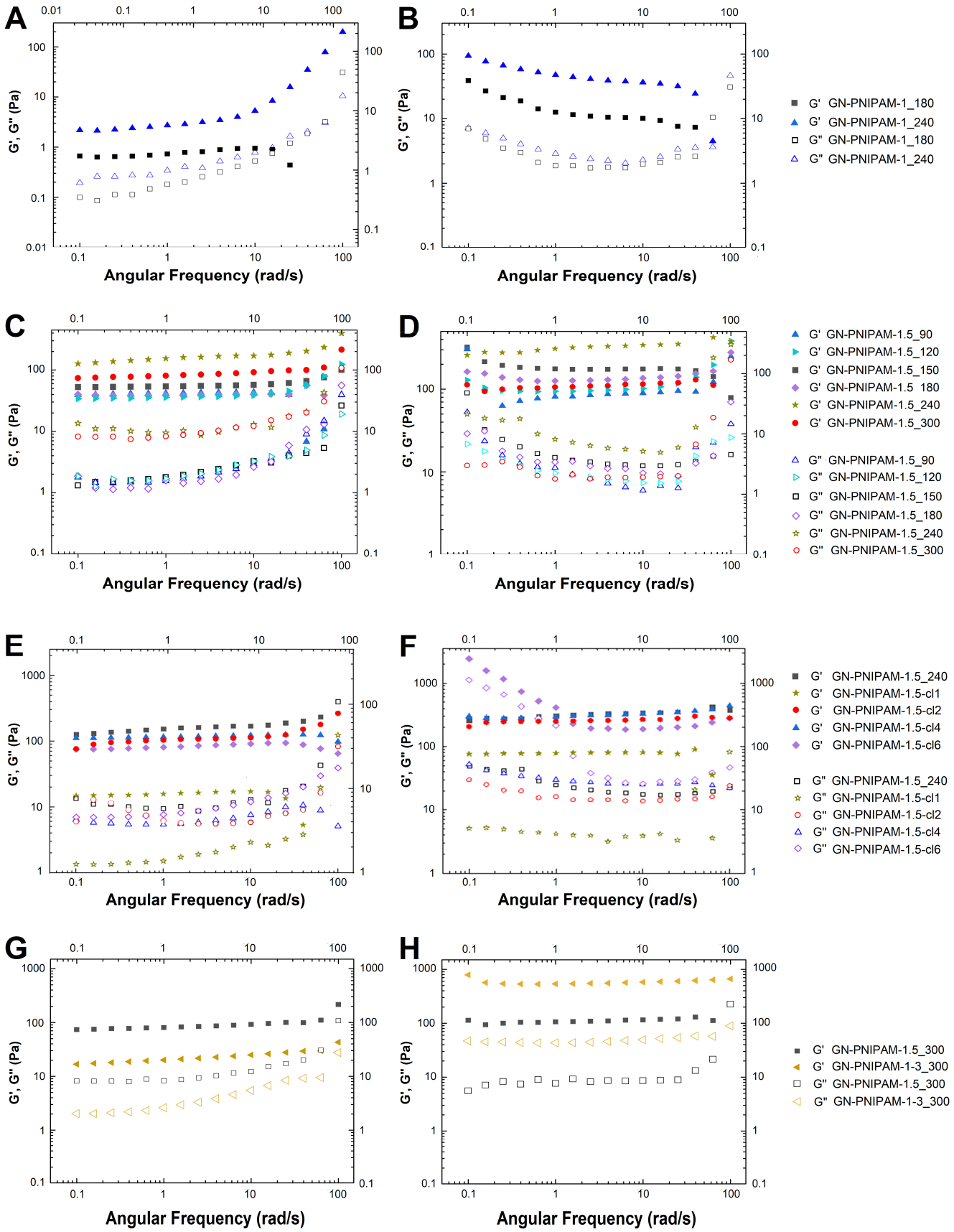

Figure 8. Amplitude strain sweeps measured for GN-PNIPAM-1 (**A**,**B**), GN-PNIPAM-1.5 (**C**,**D**), GN-PNIPAM-1.5-cl (**E**,**F**), and GN-PNIPAM-1-3 (**G**,**H**) samples at 20 °C (**A**,**C**,**E**,**G**) and 40 °C (**B**,**D**,**F**,**H**). The shear strain was 0.1% for (**A**,**B**), 0.5% for (**C**,**D**), and 1% for (**E**,**H**). Sample abbreviations corresponding to the polymerization mixture compositions are given in Table 1.

The loss modulus G″ also increased gradually but did not exceed G′ over the investigated frequency range, confirming gel-like behavior and network stability under slow and medium deformation rates (Figure 8A,C,E). At 40 °C, the trends in G′ and G″ remained similar; however, the absolute values of both moduli were substantially higher than those at 20 °C. This highlights the thermosensitive nature of the network and the strengthening of hydrophobic interactions of PNIPAM above the VPTT (Figure 8B,D,F).

For GN-PNIPAM-1.5, as the irradiation time increased from 90 to 300 s at 20 °C, a systematic increase in G′ was observed, reflecting the formation of a denser and more strongly crosslinked GN–PNIPAM network (Figure 8C). For the GN-PNIPAM-1.5-cl systems, additionally crosslinked with MBA, at 20 °C, the G′ values were close to each other and similar to the value for GN-PNIPAM-1.5 obtained without MBA, which may be attributed to a possible reduction in the effective mobility of the network (Figure 8E). At 40 °C, as the MBA content increased, the increase in G′ compared to 20 °C was most pronounced, indicating a combined enhancement in stiffness due to the thermosensitive densification of PNIPAM (Figure 8H).

When comparing the rheological properties of the GN-PNIPAM-1-3 and GN-PNIPAM-1.5 hydrogels obtained at the same irradiation time (300 s), a characteristic temperature dependence was observed. At 20 °C, G′ was higher for the system with a concentration of GN-PNIPAM-1.5 compared to GN-PNIPAM-1-3, which probably appears to be due to the more pronounced crosslinking in GN-PNIPAM-1.5 (Figure 8G). At the same time, an inversion was observed at 40 °C. For GN-PNIPAM-1-3, G′ increased sharply (~600 Pa) relative to its value at 20 °C (~20 Pa) and significantly exceeded that of GN-PNIPAM-1.5, which is attributed to the phase transition of a greater number of grafted PNIPAM chains at temperatures above the VPTT (Figure 8H).

The G′ modulus values of the obtained GN-PNIPAM hydrogels generally correspond to the elastic modulus values of certain soft tissues, for example, brain tissue (100–300 Pa) and liver tissue (400–600 Pa). The ability to be injectable at room temperature and the enhancement in mechanical properties at physiological temperature to the level of the mechanical properties of soft brain tissue, combined with the biodegradable nature of GN and the short PNIPAM chains, make such materials highly promising as implants for filling postoperative brain cavities in combination with prolonged local drug therapy.

3.3. Moxifloxacin-Loaded GN-PNIPAM Hydrogels

Moxifloxacin exhibits good water solubility. When loaded into the hydrogel matrix, it is introduced as an aqueous solution and retained within the pores of the polymer network via physical entrapment, as well as possible non-covalent interactions and hydrogen bonding with the polymer network.

The hydrogels loaded with 10 wt% MOX were studied for drug release in model conditions. Specifically, the hydrogel samples were incubated in dialysis tubes against 0.01 M PBS, pH 7.4, at 20 °C and 40 °C. During the study of the MOX release rate from GN-PNIPAM hydrogel matrices, it was found that the system exhibits pronounced temperature sensitivity and dependence on the composition of the polymer matrix (Figure 9).

According to the literature, PNIPAM-containing hydrogel systems exhibit sustained temperature-responsive release. Below the VPTT, a hydrogel swells and retains the drug; above the VPTT, it contracts, accelerating drug release [47,72]. The experimental release profiles obtained in this study are consistent with this temperature-dependent behavior. In all cases, the release curve is characterized as sustained with a noticeable burst effect at elevated temperatures during the initial stages of the process. Furthermore, the dependence of the release rate on the synthesis conditions of GN-PNIPAM is also evident. While the GN-PNIPAM-1.5, GN-PNIPAM-1.5-cl4, and GN-PNIPAM-1-3 hydrogel samples exhibited

similar release rates in the range of 38–47% over 6 days at room temperature, an increase in temperature revealed significant differences in the release rate. The lowest MOX release rate at 40 °C was observed for the GN-PNIPAM-1.5 sample (43% over 6 days), while the highest was observed for the GN-PNIPAM-1-3 sample (88% over 6 days). This result may indirectly suggest a higher content of the thermosensitive component in the GN-PNIPAM-1-3 sample, which correlates with the previously published data [73].

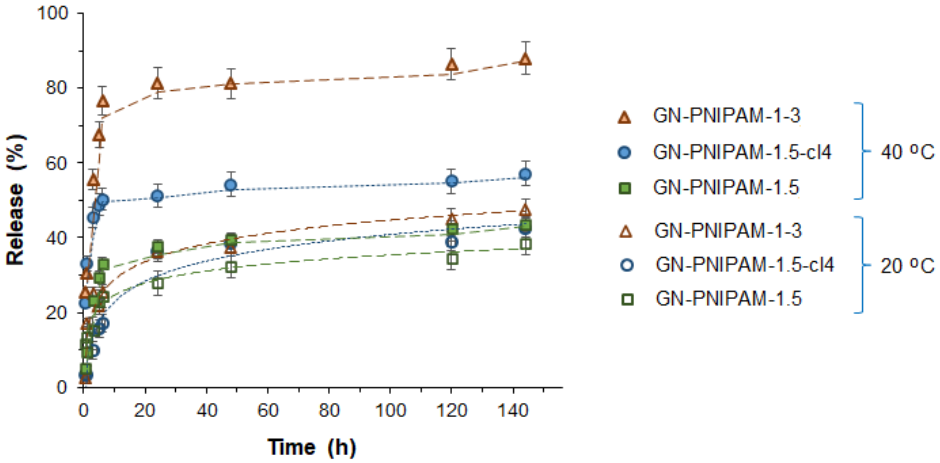

Figure 9. MOX release profiles from GN-PNIPAM hydrogels obtained under different conditions in 0.01 M PBS, pH 7.4, at 20 °C and 40 °C. *Conditions:* Samples GN-PNIPAM-1.5 and GN-PNIPAM-cl4 were synthesized under 240 s of UV irradiation. Sample GN-PNIPAM-1-3 was obtained under 480 s of UV irradiation. Sample abbreviations corresponding to the polymerization mixture compositions are given in Table 1.

Analysis of plots for MOX release from the GN-PNIPAM hydrogel matrix using various mathematical models (Table 6) showed that the highest correlation coefficients (R^2) were observed for the Korsmeyer–Peppas model. The values of the exponent *n* in the Korsmeyer–Peppas model for most samples fall within the range of 0.45–0.55. According to theory, n = 0.45–0.50 corresponds to pure Fickian diffusion (Case I), while n = 0.50–1.0 indicates anomalous diffusion (mixed mechanism) [74]. Thus, for the GN-PNIPAM-1.5-cl4 sample at 20 °C (n = 0.45) and the GN-PNIPAM-1-3 sample at 20 °C (n = 0.45), the mechanism is close to Fickian diffusion. For GN-PNIPAM-1.5-cl4 at 40 °C (n = 0.35), a decrease in the n value is observed, which may indicate faster diffusion without a significant relaxation contribution, likely due to the collapse of the polymer network above the VPTT. For GN-PNIPAM-1-3, in contrast, at 40 °C, the n value increases from 0.45 to 0.48, while the K_{KP} constant decreases slightly (from 0.13 to 0.11 min^{-1}), suggesting the mixed mechanism. For the GN-PNIPAM-1.5 sample at 20 °C (n = 0.55) and 40 °C (n = 0.52), the n values point to an anomalous diffusion mechanism.

3.4. Biological Evaluation of GN-PNIPAM Micro- and Hydrogels

The in vitro biocompatibility of the GN-PNIPAM microgel and the hydrogel samples was evaluated using human skin fibroblasts (DF2 cell line). Microgel dispersions were tested in a concentration-dependent manner (Figure 10A). Cell viability above 85% was observed for all tested samples across all concentrations. At low concentrations, evident cell proliferation was detected for all GN-containing samples, which is consistent with the known properties of gelatin [75,76].

Table 6. Results of mathematical processing of MOX release plots using several standard models.

Hydrogel *	T (°C)	Pseudo-First-Order Model		Korsmeyer–Peppas Model			Higuchi Model	
		K_1 (min^{-1})	R^2	K_{KP} (min^{-1})	n	R^2	K_H ($min^{-0.5}$)	R^2
GN-PNIPAM-1.5-cl4	20	0.021	0.9515	0.09	0.45	0.9646	0.08	0.9537
	40	0.015	0.9543	0.41	0.35	0.9634	0.47	0.9545
GN-PNIPAM-1-3	20	0.015	0.9538	0.13	0.45	0.9598	0.19	0.9454
	40	0.030	0.9346	0.11	0.48	0.9698	0.22	0.9555
GN-PNIPAM-1.5	20	0.050	0.9235	0.16	0.55	0.9648	0.28	0.9421
	40	0.045	0.9025	0.18	0.52	0.9432	0.30	0.9185

* Sample abbreviations corresponding to the polymerization mixture compositions are given in Table 1.

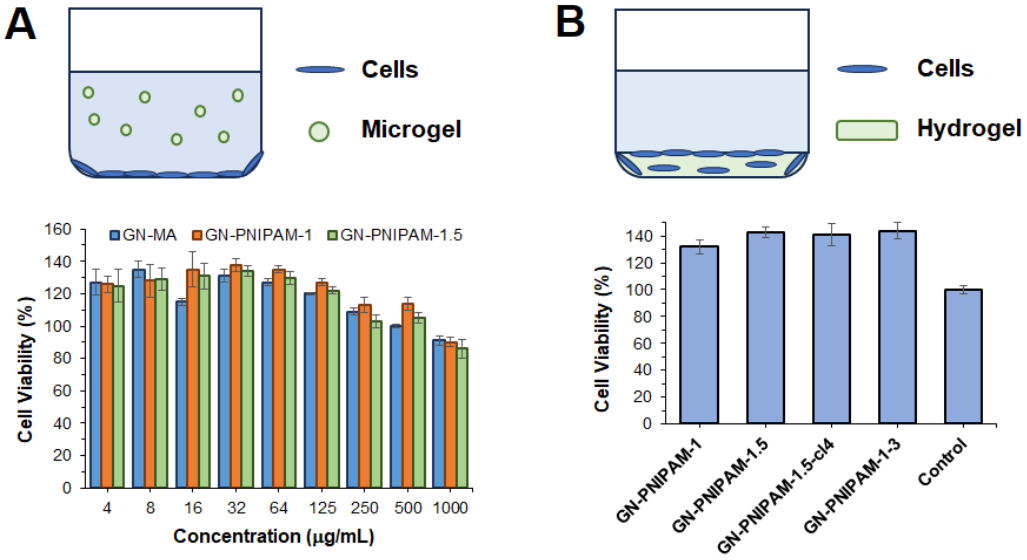

Figure 10. Cytotoxicity of GN-PNIPAM microgels (**A**) and GN-PNIPAM hydrogel layers (**B**) in human skin fibroblasts (DF2 cell line, 72 h, MTT assay). Sample abbreviations corresponding to the polymerization mixture compositions are given in Table 1.

In the case of the hydrogels, cells were seeded onto the surfaces of hydrogel coatings previously formed at the bottom of the plate wells (Figure 10B). The plastic bottom of the wells was used as a control surface. The results demonstrate high biocompatibility of the cells with the hydrogel matrices. The higher viability observed for all hydrogels can be attributed to the differences in the space available for cell growth. Whereas the control surface provides a two-dimensional (2D) environment, the hydrogel layers offer a three-dimensional (3D) architecture. Active cell proliferation and high viability in the GN-PNIPAM hydrogels after 72 h indicate that the hydrogels provide a cell-friendly environment. At the same time, no drastic differences in cell behavior were observed depending on the hydrogel composition.

4. Conclusions

In this study, the photopolymerization of GN-MA with NIPAM yielded GN-PNIPAM microgels. The effects of monomer concentration, crosslinker content (MBA), and irradiation time on product yield, grafted chain length, and material properties were systematically investigated. At a low NIPAM concentration (1 wt%), a high product yield (>90%) was achieved after irradiation starting at 180 s. Kinetic analysis revealed that at higher NIPAM concentrations, more frequent radical encounters increase the number of grafted chains but also promote homopolymerization, thereby increasing irradiation time and reducing

the target product yield. At intermediate concentrations (1.5 wt% GN-MA together with 1.5 wt% NIPAM), the length of grafted PNIPAM chains extends as a result of diffusionally limiting termination impact due to increased viscosity of the polymerization mixture as well as reduced side homopolymrization processes. The introduction of the crosslinker (MBA, 0.025–0.50 wt%) increased the GN-PNIPAM-1.5 yield. In all cases, the grafted PNIPAM chains were quite short (M_n < 2000), meaning that after gelatin degradation, they will not be limited in their removal from the body. Despite the high monomer conversion, it was not complete. To exclude the effect of the monomer on the physicochemical and biological properties of the micro- and hydrogels, the samples were carefully purified of low-molecular-weight impurities by dialysis.

All microgels demonstrated about a twofold decrease in hydrodynamic diameter upon transition from 20 °C to 40 °C. An MBA content of 0.5 wt% provided superior swelling capacity and the most pronounced thermosensitive volume collapse, with a fivefold reduction in hydrodynamic diameter upon heating. This can be explained by an optimal number of crosslinks, providing a robust and elastic network that cooperatively and uniformly expels water, leading to a strong and synchronized collapse at temperatures above the VPTT. Rheological analysis confirmed viscoelastic behavior with the increase in the storage modulus (G') exceeding the loss modulus (G'') across all frequencies. The elastic moduli ranged from 20 to 600 Pa, matching those of soft tissues, such as the brain (100–300 Pa) and liver (400–600 Pa). This suggests injectability at room temperature and mechanical reinforcement at physiological temperature. Moxifloxacin release was temperature-dependent and followed the Korsmeyer–Peppas model with predominantly Fickian diffusion; release rates varied from 38% to 88% over 6 days, with the highest release observed for the GN-PNIPAM-1–3 sample due to its higher content of the thermosensitive component. Finally, all microgel and hydrogel samples demonstrated excellent biocompatibility (>85% cell viability) with human skin fibroblasts, and active cell proliferation on the hydrogel surfaces confirmed a cell-friendly three-dimensional environment.

Overall, the developed GN-PNIPAM hydrogels combine the biodegradability of GN, the thermosensitivity of PNIPAM, tunable mechanical properties, and excellent biocompatibility. These features make them promising candidates for biomedical applications, particularly as injectable implants for postoperative cavity filling in soft tissues with prolonged and stimuli-responsive local drug delivery.

Supplementary Materials: The following supporting information can be downloaded at https://www.mdpi.com/article/10.3390/macromol6020034/s1, Figure S1: ^{1}H NMR spectrum of GN-MA; Figure S2: DSC thermograms of hydrogels: (A) GN-PNIPAM-1_180, (B) GN-PNIPAM-1_240, (C) GN-PNIPAM-1.5_240, and (D) GN-PNIPAM-1-3_480.

Author Contributions: Conceptualization, O.L. and E.K.-V.; methodology, O.L., E.S. and Y.N.; formal analysis, O.L., E.S. and E.K.-V.; investigation, O.L., E.S., I.B., O.S., A.N., Y.N. and V.I.; resources, O.L., Y.N., E.S. and E.K.-V.; data curation, O.L., E.S. and Y.N.; writing—original draft preparation, O.L. and E.K.-V.; writing—review and editing, E.S. and E.K.-V.; visualization, O.L. and E.K.-V.; supervision, E.K.-V.; project administration, O.L.; funding acquisition, O.L. All authors have read and agreed to the published version of the manuscript.

Funding: This study was supported by the Russian Science Foundation (project #25-73-00379).

Institutional Review Board Statement: Not applicable.

Data Availability Statement: The raw data supporting the conclusions of this article will be made available by the authors on request.

Acknowledgments: The Interdisciplinary Resource Centre for Nanotechnology of the Research Park of SPbU is gratefully acknowledged.

Conflicts of Interest: The authors declare no conflicts of interest.

Abbreviations

The following abbreviations are used in this manuscript:

LCST	Lower critical solution temperature
UCST	Upper critical solution temperature
VPTT	Volume phase transition temperature
GN	Gelatin
GM-MA	Methacrylated gelatin
NIPAM	*N*-isopropylacrylamide
PNIPAM	Poly(*N*-isopropylacrylamide)
MBA	*N*,*N*′-methylenebisacrylamide
GN-PNIPAM	Graft copolymer obtained via photoinduced copolymerization of GN-MA and NIPAM
GN-PNIPAM-cl	Graft copolymer obtained via photoinduced copolymerization of GN-MA and NIPAM additionally cross-linked with MBA
MOX	Moxifloxacin

References

1. Alexander, A.; Ajazuddin; Khan, J.; Saraf, S.; Saraf, S. Polyethylene glycol (PEG)–Poly(N-isopropylacrylamide) (PNIPAAm) based thermosensitive injectable hydrogels for biomedical applications. *Eur. J. Pharm. Biopharm.* **2014**, *88*, 575–585. [CrossRef] [PubMed]
2. Singhal, R.; Sarangi, M.K.; Rath, G. Injectable Hydrogels: A Paradigm Tailored with Design, Characterization, and Multifaceted Approaches. *Macromol. Biosci.* **2024**, *24*, 2400049. [CrossRef]
3. Simpson, C.R.; Kelly, H.M.; Murphy, C.M. The Design and Development of an Injectable Thermoresponsive Hydrogel for Controlled Simvastatin Release in Bone Repair Applications. *Gels* **2025**, *11*, 995. [CrossRef]
4. Bellotti, E.; Schilling, A.L.; Little, S.R.; Decuzzi, P. Injectable thermoresponsive hydrogels as drug delivery system for the treatment of central nervous system disorders: A review. *J. Control. Release* **2021**, *329*, 16–35. [CrossRef]
5. Ding, Y.; Zhang, X.; Xu, B.; Li, W. LCST and UCST-type thermoresponsive behavior in dendronized gelatins. *Polym. Chem.* **2022**, *13*, 2813–2821. [CrossRef]
6. Tang, L.; Liu, F.; Xu, Y.; Xiao, D.; Zhang, Z.; Jiang, H.; Gong, L.; Tang, J. Highly Bidirectional Actuation of LCST- and UCST-Type Bilayer Hydrogel Actuators with Enhanced Mechanical Properties and Interfacial Toughness. *ACS Appl. Polym. Mater.* **2025**, *7*, 2819–2829. [CrossRef]
7. Zhao, H.; An, H.; Xi, B.; Yang, Y.; Qin, J.; Wang, Y.; He, Y.; Wang, X. Self-Healing Hydrogels with both LCST and UCST through Cross-Linking Induced Thermo-Response. *Polymers* **2019**, *11*, 490. [CrossRef]
8. Lupu, A.; Bercea, M.; Avadanei, M.; Gradinaru, L.M.; Nita, L.E.; Gradinaru, V.R. Temperature Sensitive Pluronic F127-Based Gels Incorporating Natural Therapeutic Agents. *Macromol. Mater. Eng.* **2025**, *310*, 2400341. [CrossRef]
9. Marsili, L.; Dal Bo, M.; Eisele, G.; Donati, I.; Berti, F.; Toffoli, G. Characterization of Thermoresponsive Poly-N-Vinylcaprolactam Polymers for Biological Applications. *Polymers* **2021**, *13*, 2639. [CrossRef]
10. Singh, A.; Dowdall, N.; Hoare, T. Poly(Oligo(Ethylene Glycol) Methacrylate)-Based Polymers in Biomedical Applications: Preparation and Applications. *Biomacromolecules* **2025**, *26*, 3929–3973. [CrossRef] [PubMed]
11. Lusina, A.; Nazim, T.; Cegłowski, M. Poly(2-oxazoline)s as Stimuli-Responsive Materials for Biomedical Applications: Recent Developments of Polish Scientists. *Polymers* **2022**, *14*, 4176. [CrossRef]
12. Lanzalaco, S.; Mingot, J.; Torras, J.; Alemán, C.; Armelin, E. Recent Advances in Poly(N-isopropylacrylamide) Hydrogels and Derivatives as Promising Materials for Biomedical and Engineering Emerging Applications. *Adv. Eng. Mater.* **2023**, *25*, 2201303. [CrossRef]
13. Movaffagh, J.; Hadizadeh, F.; Khodaverdi, E.; Khalili, B.; Rezaeian Shiadeh, S.N.; Kamali, H.; Oroojalian, F. Preparation and in vitro evaluation of injectable formulations of levothyroxine sodium using in situ forming hydrogel temperature-responsive systems based on PLA-PEG-PLA and PLGA-PEG-PLGA triblock copolymers. *Iran. J. Basic Med. Sci.* **2022**, *25*, 341–351.
14. Heine, S.; Aguilar-Pimentel, A.; Russkamp, D.; Alessandrini, F.; Gailus-Durner, V.; Fuchs, H.; Ollert, M.; Bredehorst, R.; Ohnmacht, C.; Zissler, U.M.; et al. Thermosensitive PLGA–PEG–PLGA Hydrogel as Depot Matrix for Allergen-Specific Immunotherapy. *Pharmaceutics* **2022**, *14*, 1527. [CrossRef]
15. Vdovchenko, A.A.; Hubina, A.V.; Vlakh, E.G.; Tennikova, T.B. Self-assembled polymer particles based on thermoresponsive biodegradable copolymers of amino acids. *Mendeleev Commun.* **2017**, *27*, 153–154. [CrossRef]

16. Tarasenko, I.I.; Zakharova, N.N.; Vlasova, E.N.; Korzhikova-Vlakh, E.G. A novel thermoresponsive polypeptide: Synthesis and characterization. *Mendeleev Commun.* **2024**, *34*, 348–350. [CrossRef]
17. Liu, D.; Sun, J. Thermoresponsive Polypeptoids. *Polymers* **2020**, *12*, 2973. [CrossRef]
18. Moon, S.H.; Park, S.J.; Lee, Y.W.; Yang, Y.J. LCST/UCST behavior of polysaccharides for hydrogel fabrication. *RSC Adv.* **2024**, *14*, 35754–35768. [CrossRef] [PubMed]
19. Chen, L.; Honma, Y.; Mizutani, T.; Liaw, D.-J.; Gong, J.; Osada, Y. Effects of polyelectrolyte complexation on the UCST of zwitterionic polymer. *Polymer* **2000**, *41*, 141–147. [CrossRef]
20. Wu, Z.; Fan, J.; Hu, J.; Xie, W.; Sun, S.; Hu, S.; Li, C.; Wang, Z.; Ituen, E. Temperature-responsive salt-resistant poly(sulfobetaine methacrylate)-based emulsifiers for heavy oils. *Int. J. Biol. Macromol.* **2024**, *268*, 131977. [CrossRef] [PubMed]
21. Eckert, T.; Abetz, V. Polymethacrylamide—An underrated and easily accessible upper critical solution temperature polymer: Green synthesis via photoiniferter reversible addition–fragmentation chain transfer polymerization and analysis of solution behavior in water/ethanol mixtu. *J. Polym. Sci.* **2020**, *58*, 3050–3060. [CrossRef]
22. Kuroyanagi, S.; Shimada, N.; Fujii, S.; Furuta, T.; Harada, A.; Sakurai, K.; Maruyama, A. Highly Ordered Polypeptide with UCST Phase Separation Behavior. *J. Am. Chem. Soc.* **2019**, *141*, 1261–1268.
23. Xu, Z.; Liu, W. Poly(N-acryloyl glycinamide): A fascinating polymer that exhibits a range of properties from UCST to high-strength hydrogels. *Chem. Commun.* **2018**, *54*, 10540–10553. [CrossRef]
24. Pham, Q.-T.; Yao, Z.-H.; Chang, Y.-T.; Wang, F.-M.; Chern, C.-S. LCST phase transition kinetics of aqueous poly(N-isopropylacrylamide) solution. *J. Taiwan Inst. Chem. Eng.* **2018**, *93*, 63–69. [CrossRef]
25. Throat, S.; Bhattacharya, S. Macromolecular Poly(N-isopropylacrylamide) (PNIPAM) in Cancer Treatment and Beyond. *Adv. Polym. Technol.* **2024**, *2024*, 1444990.
26. Cohen, N. Phase Coexistence in Thermoresponsive PNIPAM Hydrogels Triggered by Mechanical Forces. *Macromolecules* **2026**, *59*, 2580–2589. [CrossRef] [PubMed]
27. Lanzalaco, S.; Armelin, E. Poly(N-isopropylacrylamide) and Copolymers: A Review on Recent Progresses in Biomedical Applications. *Gels* **2017**, *3*, 36. [CrossRef] [PubMed]
28. Jain, K.; Vedarajan, R.; Watanabe, M.; Ishikiriyama, M.; Matsumi, N. Tunable LCST behavior of poly(N-isopropylacrylamide/ionic liquid) copolymers. *Polym. Chem.* **2015**, *6*, 6819–6825. [CrossRef]
29. Rzaev, Z.M.O.; Dinçer, S.; Pişkin, E. Functional copolymers of N-isopropylacrylamide for bioengineering applications. *Prog. Polym. Sci.* **2007**, *32*, 534–595. [CrossRef]
30. Pilipenko, I.; Korzhikov-Vlakh, V.; Valtari, A.; Anufrikov, Y.; Kalinin, S.; Ruponen, M.; Krasavin, M.; Urtti, A.; Tennikova, T. Mucoadhesive properties of nanogels based on stimuli-sensitive glycosaminoglycan-graft-pNIPAAm copolymers. *Int. J. Biol. Macromol.* **2021**, *186*, 864–872.
31. Pilipenko, I.M.; Korzhikov-Vlakh, V.A.; Zakharova, N.V.; Urtti, A.; Tennikova, T.B. Thermo- and pH-sensitive glycosaminoglycans derivatives obtained by controlled grafting of poly(N-isopropylacrylamide). *Carbohydr. Polym.* **2020**, *248*, 116764. [CrossRef]
32. Pei, Y.; Chen, J.; Yang, L.; Shi, L.; Tao, Q.; Hui, B.; Li, J. The effect of pH on the LCST of poly(N-isopropylacrylamide) and poly(N-isopropylacrylamide-co-acrylic acid). *J. Biomater. Sci. Polym. Ed.* **2004**, *15*, 585–594. [CrossRef]
33. Pastoor, K.J.; Rice, C.V. Cation Effects on the Phase Transition of *N*-isopropylacrylamide Hydrogels. *Macromol. Chem. Phys.* **2015**, *216*, 1024–1032. [CrossRef]
34. Ciarleglio, G.; Toto, E.; Santonicola, M.G. Conductive and Thermo-Responsive Composite Hydrogels with Poly(N-isopropylacrylamide) and Carbon Nanotubes Fabricated by Two-Step Photopolymerization. *Polymers* **2023**, *15*, 1022. [CrossRef] [PubMed]
35. Bischofberger, I.; Calzolari, D.C.E.; De Los Rios, P.; Jelezarov, I.; Trappe, V. Hydrophobic hydration of poly-N-isopropyl acrylamide: A matter of the mean energetic state of water. *Sci. Rep.* **2014**, *4*, 4377. [CrossRef] [PubMed]
36. Li, H.; Sun, H.; Liu, Y.; Yuan, B.; Hu, J.; Jiang, Y.; Li, Q.; Cao, S.; Liu, H.; Xiao, B.; et al. Toxicology and safety research of poly(N-isopropylacrylamide)-based thermosensitive nanogels. *Environ. Sci. Nano* **2023**, *10*, 3357–3365.
37. Cooperstein, M.A.; Canavan, H.E. Assessment of cytotoxicity of (N-isopropyl acrylamide) and Poly(N-isopropyl acrylamide)-coated surfaces. *Biointerphases* **2013**, *8*, 19.
38. Mohanto, S.; Narayana, S.; Merai, K.P.; Kumar, J.A.; Bhunia, A.; Hani, U.; Al Fatease, A.; Gowda, B.H.J.; Nag, S.; Ahmed, M.G.; et al. Advancements in gelatin-based hydrogel systems for biomedical applications: A state-of-the-art review. *Int. J. Biol. Macromol.* **2023**, *253*, 127143.
39. Hong, S.-J.; Kim, D.-H.; Ryoo, J.-H.; Park, S.-M.; Kwon, H.-C.; Keum, D.-H.; Shin, D.-M.; Han, S.-G. Influence of Gelatin on Adhesion, Proliferation, and Adipogenic Differentiation of Adipose Tissue-Derived Stem Cells Cultured on Soy Protein–Agarose Scaffolds. *Foods* **2024**, *13*, 2247.
40. Li, M.; Wu, C. Self-Association of Poly(N-isopropylacrylamide) and Its Complexation with Gelatin in Aqueous Solution. *Macromolecules* **1999**, *32*, 4311–4316. [CrossRef]

41. Ohya, S.; Nakayama, Y.; Matsuda, T. Material design for an artificial extracellular matrix: Cell entrapment in poly (N-isopropylacrylamide) (PNIPAM)-grafted gelatin hydrogel. *J. Artif. Organs* **2001**, *4*, 308–314. [CrossRef]
42. Ohya, S.; Kidoaki, S.; Matsuda, T. Poly(N-isopropylacrylamide) (PNIPAM)-grafted gelatin hydrogel surfaces: Interrelationship between microscopic structure and mechanical property of surface regions and cell adhesiveness. *Biomaterials* **2005**, *26*, 3105–3111. [CrossRef]
43. Boudet, C.; Iliopoulos, I.; Monti, F.; Cloitre, M.; Poncelet, O. Smart Reactivity in Gelatine/PNIPAM Mixtures: Control of the Cross-Linking and Microheterogeneities. *Macromol. Symp.* **2006**, *239*, 114–119. [CrossRef]
44. Tsai, F.-C.; Huang, C.-F.; Chang, C.-J.; Lu, C.-H.; Chen, J.-K. Thermo-Tunable Pores and Antibiotic Gating Properties of Bovine Skin Gelatin Gels Prepared with Poly(n-isopropylacrylamide) Network. *Polymers* **2020**, *12*, 2156. [CrossRef]
45. Parvathy, P.A.; De, S.; Singh, M.; Manik, G.; Sahoo, S.K. Functional self-healing aldehyde-derived nanoparticle-crosslinked gelatin/PNIPAm-based adhesive gels. *RSC Appl. Polym.* **2025**, *3*, 662–674. [CrossRef]
46. Lee, J.M.; Ma, W.C.; Yeong, W.Y. Dual-hydrogel thermoresponsive system with bioinspired pore control for drug delivery. *Next Mater.* **2025**, *6*, 100281. [CrossRef]
47. Daaboul, M.; Akkaya, A.; Kanli, Z.; Gunduz, O.; Aydın, B.; Alarcin, E.; Ozmen, M.M.; Topuzogullari, M. Nanoparticle-Embedded GelMA/NIPAm Hydrogels: A Temperature-Responsive Hybrid System for Controlled Drug Release. *Macromol. Biosci.* **2026**, *26*, e00635. [CrossRef]
48. Sengupta, P.; Salisbury, E.; Kumar, A.; Junkers, T.; Cameron, N.R. Production of gelatin methacrylate by flow chemistry and investigation of its suitability as a biomaterial. *RSC Appl. Polym.* **2025**, *3*, 1204–1215. [CrossRef]
49. Liu, X.; Yang, J.; Zha, L.; Jiang, Z. Self-assembly of hollow PNIPAM microgels to form discontinuously hollow fibers. *Chin. J. Polym. Sci.* **2014**, *32*, 1544–1549. [CrossRef]
50. Lalji, S.M.; Ali, S.I.; Ahmed, R.; Hashmi, S.; Awan, Z.U.H. Comparative performance analysis of different swelling kinetic models for the evaluation of shale swelling. *J. Pet. Explor. Prod. Technol.* **2022**, *12*, 1237–1249. [CrossRef]
51. Blanco, A.; González, G.; Casanova, E.; Pirela, M.E.; Briceño, A. Mathematical Modeling of Hydrogels Swelling Based on the Finite Element Method. *Appl. Math.* **2013**, *4*, 161–170. [CrossRef]
52. Thirupathi, K.; Phan, T.T.V.; Santhamoorthy, M.; Ramkumar, V.; Kim, S.-C. pH and Thermoresponsive PNIPAm-co-Polyacrylamide Hydrogel for Dual Stimuli-Responsive Controlled Drug Delivery. *Polymers* **2022**, *15*, 167. [CrossRef]
53. Coughlan, D.C.; Quilty, F.P.; Corrigan, O.I. Effect of drug physicochemical properties on swelling/deswelling kinetics and pulsatile drug release from thermoresponsive poly(N-isopropylacrylamide) hydrogels. *J. Control. Release* **2004**, *98*, 97–114. [CrossRef]
54. Vigata, M.; Meinert, C.; Hutmacher, D.W.; Bock, N. Hydrogels as Drug Delivery Systems: A Review of Current Characterization and Evaluation Techniques. *Pharmaceutics* **2020**, *12*, 1188. [CrossRef]
55. Costa, P.; Sousa Lobo, J.M. Modeling and comparison of dissolution profiles. *Eur. J. Pharm. Sci.* **2001**, *13*, 123–133. [CrossRef] [PubMed]
56. Monteiro, N.; Thrivikraman, G.; Athirasala, A.; Tahayeri, A.; França, C.M.; Ferracane, J.L.; Bertassoni, L.E. Photopolymerization of cell-laden gelatin methacryloyl hydrogels using a dental curing light for regenerative dentistry. *Dent. Mater.* **2018**, *34*, 389–399. [CrossRef] [PubMed]
57. Xu, X.; Liu, Y.; Fu, W.; Yao, M.; Ding, Z.; Xuan, J.; Li, D.; Wang, S.; Xia, Y.; Cao, M. Poly(N-isopropylacrylamide)-Based Thermoresponsive Composite Hydrogels for Biomedical Applications. *Polymers* **2020**, *12*, 580. [CrossRef]
58. Zhu, X.; Gu, X.; Zhang, L.; Kong, X.-Z. Preparation and characterization of nanosized P(NIPAM-MBA) hydrogel particles and adsorption of bovine serum albumin on their surface. *Nanoscale Res. Lett.* **2012**, *7*, 519. [CrossRef]
59. Schlattmann, D.; Schönhoff, M. Interplay of the Influence of Crosslinker Content and Model Drugs on the Phase Transition of Thermoresponsive PNiPAM-BIS Microgels. *Gels* **2022**, *8*, 571. [CrossRef] [PubMed]
60. Syamjith, K.S.; Rout, S.; Jacob, A.R. Revisiting crosslinking density effects on pNIPAM microgel properties: Size, electrophoretic mobility, and transition temperatures. *J. Chem. Phys.* **2025**, *162*, 184903. [CrossRef]
61. Burmistrova, A.; Richter, M.; Eisele, M.; Üzüm, C.; Von Klitzing, R. The Effect of Co-Monomer Content on the Swelling/Shrinking and Mechanical Behaviour of Individually Adsorbed PNIPAM Microgel Particles. *Polymers* **2011**, *3*, 1575–1590. [CrossRef]
62. Bandyopadhyay, S.; Sharma, A.; Ashfaq Alvi, M.A.; Raju, R.; Glomm, W.R. A robust method to calculate the volume phase transition temperature (VPTT) for hydrogels and hybrids. *RSC Adv.* **2017**, *7*, 53192–53202. [CrossRef]
63. Kyrey, T.; Witte, J.; Lutzki, J.; Zamponi, M.; Wellert, S.; Holderer, O. Mobility of bound water in PNIPAM microgels. *Phys. Chem. Chem. Phys.* **2021**, *23*, 14252–14259. [CrossRef]
64. Gun'ko, V.; Savina, I.; Mikhalovsky, S. Properties of Water Bound in Hydrogels. *Gels* **2017**, *3*, 37. [CrossRef]
65. Futscher, M.H.; Philipp, M.; Müller-Buschbaum, P.; Schulte, A. The Role of Backbone Hydration of Poly(N-isopropyl acrylamide) Across the Volume Phase Transition Compared to its Monomer. *Sci. Rep.* **2017**, *7*, 17012. [CrossRef]
66. Chang, C.-W.; Dargaville, B.L.; Momot, K.I.; Hutmacher, D.W. An investigation of water status in gelatin methacrylate hydrogels by means of water relaxometry and differential scanning calorimetry. *J. Mater. Chem. B* **2024**, *12*, 6328–6341. [CrossRef] [PubMed]

67. Vigata, M.; Meinert, C.; Bock, N.; Dargaville, B.L.; Hutmacher, D.W. Deciphering the Molecular Mechanism of Water Interaction with Gelatin Methacryloyl Hydrogels: Role of Ionic Strength, pH, Drug Loading and Hydrogel Network Characteristics. *Biomedicines* **2021**, *9*, 574. [CrossRef] [PubMed]
68. Tamminen, A.; Baggio, M.; Grigorev, R.; Nefedova, I.; Pälli, S.V.; Ala-Laurinaho, J.; Brown, E.R.; Wallace, V.P.; MacPherson, E.; Maloney, T.; et al. Characterization of bound and free water in gelatin hydrogels and their contribution to THz frequency permittivity. In Proceedings of the 2022 47th International Conference on Infrared, Millimeter and Terahertz Waves (IRMMW-THz), Delft, The Netherlands, 28 August–2 September 2022; pp. 1–2.
69. Rodríguez-Rodríguez, R.; García-Carvajal, Z.Y.; Jiménez-Palomar, I.; Jiménez-Avalos, J.A.; Espinosa-Andrews, H. Development of gelatin/chitosan/PVA hydrogels: Thermal stability, water state, viscoelasticity, and cytotoxicity assays. *J. Appl. Polym. Sci.* **2019**, *136*, 47149. [CrossRef]
70. Ikeda-Fukazawa, T.; Ikeda, N.; Tabata, M.; Hattori, M.; Aizawa, M.; Yunoki, S.; Sekine, Y. Effects of crosslinker density on the polymer network structure in poly-*N*,*N*-dimethylacrylamide hydrogels. *J. Polym. Sci. Part B Polym. Phys.* **2013**, *51*, 1017–1027. [CrossRef]
71. Buratti, E.; Sguizzato, M.; Sotgiu, G.; Zamboni, R.; Bertoldo, M. Keratin–PNIPAM Hybrid Microgels: Preparation, Morphology and Swelling Properties. *Gels* **2024**, *10*, 411. [CrossRef]
72. Viola, M.; Valverde, M.G.; Bernal, P.N.; van Trijp, J.P.; Hak, J.; Di Marco, G.; Neumann, M.; Schuurmans, C.C.L.; van Nostrum, C.F.; Masereeuw, R.; et al. Thermal Shrinking of Biopolymeric Hydrogels for High Resolution 3D Printing of Kidney Tubules. *Adv. Funct. Mater.* **2024**, *34*, 2406098. [CrossRef]
73. Trongsatitkul, T.; Budhlall, B.M. Microgels or microcapsules? Role of morphology on the release kinetics of thermoresponsive PNIPAm-co-PEGMa hydrogels. *Polym. Chem.* **2013**, *4*, 1502–1516. [CrossRef]
74. Ritger, P.L.; Peppas, N.A. A simple equation for description of solute release II. Fickian and anomalous release from swellable devices. *J. Control. Release* **1987**, *5*, 37–42. [CrossRef]
75. Yang, G.; Xiao, Z.; Long, H.; Ma, K.; Zhang, J.; Ren, X.; Zhang, J. Assessment of the characteristics and biocompatibility of gelatin sponge scaffolds prepared by various crosslinking methods. *Sci. Rep.* **2018**, *8*, 1616. [CrossRef] [PubMed]
76. Sung, B.; Krieger, J.; Yu, B.; Kim, M. Colloidal gelatin microgels with tunable elasticity support the viability and differentiation of mesenchymal stem cells under pro-inflammatory conditions. *J. Biomed. Mater. Res. Part A* **2018**, *106*, 2753–2761. [CrossRef]